

Anatomy of Exotic Higgs Decays in 2HDM

Felix Kling,^{a,b} Jose Miguel No,^c Shufang Su^a

^a*Department of Physics, University of Arizona, Tucson, Arizona 85721, USA*

^b*Fermilab, P.O. Box 500, Batavia, IL 60510, USA*

^c*Department of Physics and Astronomy, University of Sussex, Brighton, BN1 9QH, UK*

E-mail: kling@email.arizona.edu, J.M.No@sussex.ac.uk,
shufang@email.arizona.edu

ABSTRACT: Large mass splittings between new scalars in two-Higgs-doublet models (2HDM) open a key avenue to search for these new states via exotic heavy Higgs decays. We discuss in detail the different search channels for these new scalars at the LHC in the presence of a sizable mass splitting, *i.e.* a hierarchical 2HDM scenario, taking into account the theoretical and experimental constraints. We provide benchmark planes to exploit the complementarity among these searches, analyzing their potential to probe the hierarchical 2HDM parameter space during LHC Run 2.

Contents

| | | |
|----------|---|-----------|
| 1 | Introduction | 2 |
| 2 | Two Higgs Doublet Models: A Review | 3 |
| 2.1 | 2HDM Lagrangian and Higgs Potential | 3 |
| 2.2 | Interactions in the 2HDM | 4 |
| 2.3 | The Alignment Limit and the Role of m_{12}^2 | 5 |
| 3 | 2HDM Theoretical and Experimental Constraints | 6 |
| 3.1 | Vacuum Stability | 6 |
| 3.2 | Perturbativity and Unitarity | 7 |
| 3.3 | Electroweak Precision Measurements | 8 |
| 3.4 | Flavour Constraints | 9 |
| 3.5 | LHC and LEP Constraints | 9 |
| 3.6 | From Constraints to 2HDM Benchmarks | 10 |
| 4 | LHC Production and Decay of 2HDM Higgses | 11 |
| 5 | 2HDM Planes for Exotic Higgs Decays | 14 |
| 5.1 | Exotic Decays in the Alignment Limit | 17 |
| 5.1.1 | BP IA: $m_A > m_H = m_{H^\pm}$ | 17 |
| 5.1.2 | BP IIB: $m_H < m_A = m_{H^\pm}$ | 18 |
| 5.1.3 | BP IB: $m_A < m_{H^\pm} = m_H$ | 19 |
| 5.1.4 | BP IIA: $m_H > m_A = m_{H^\pm}$ | 20 |
| 5.2 | Exotic Decays into h Away from Alignment | 20 |
| 5.2.1 | BP III: $m_A = m_H = m_{H^\pm}$ vs. $c_{\beta-\alpha}$ | 20 |
| 6 | Conclusions | 23 |
| A | Production Cross Sections and Branching Ratios of 2HDM Higgses | 26 |
| A.1 | 2HDM Production Cross Sections | 26 |
| A.2 | 2HDM Branching Ratios for Exotic Higgs Decays | 26 |

1 Introduction

Analyses of the results from the LHC 7-8 TeV run by both ATLAS and CMS show that the properties of the Higgs particle at $m_h \sim 125$ GeV are close to those expected for the Standard Model (SM) Higgs boson h_{SM} [1, 2]. The complete nature of the scalar sector responsible for electroweak (EW) symmetry-breaking, however, remains to be determined, and it is particularly interesting to ascertain whether the Higgs sector consists of only one $\text{SU}(2)_L$ scalar doublet or has a richer structure containing additional states. Addressing this question is a key task for present and future studies at the Large Hadron Collider (LHC).

Two Higgs doublet models (2HDM) constitute the prime example of a well-motivated extended Higgs sector, appearing in many extensions of the SM such as the MSSM [3], composite Higgs models [4] and viable EW baryogenesis scenarios [5]. In addition to the SM-like CP-even Higgs boson, the 2HDM spectrum contains one more CP-even Higgs, a CP-odd Higgs and a pair of charged ones*. In recent years, its allowed parameter space has been scrutinized in light of ATLAS/CMS Higgs coupling measurements and searches for extra Higgses at the LHC [6–15].

A key avenue to probe the 2HDM heavy Higgs bosons at the LHC which has started to attract attention recently is the search for exotic decays of the heavy Higgses in the presence of a sizable mass splitting among them [16–21] (see also [15]). These sizable splittings are difficult to realize in the MSSM, while in more general 2HDM scenarios they may lead to important physical consequences†. While the conventional decay channels of a heavy Higgs into two SM quarks, leptons or gauge bosons have been the focus of most of the existing searches, the exotic (non-SM) modes of a heavy Higgs decaying into two light Higgses, or one light Higgs with one SM gauge boson quickly dominate once they are kinematically open. The current exclusion bounds on extra Higgses based on their conventional decays only will be therefore significantly relaxed. On the other hand, the exotic decay modes offer new discovery channels, which have already shown exclusion power during the 8 TeV LHC run [22, 23], and yield very promising prospects for the 13 TeV LHC run. In this work, we aim to provide a comprehensive categorization and analysis of the exotic search channels for the new 2HDM scalars, highlighting the complementarity among them, and provide guiding benchmark planes for Run 2 of the LHC at 13 TeV.

After a review of the 2HDM in Section 2, we present the constraints on the 2HDM parameter space coming from theoretical considerations (stability of the EW minimum, perturbativity and tree-level unitarity) and experimental measurements in Section 3, where we also introduce the salient features of our benchmark scenarios for exotic 2HDM Higgs decays (Section 3.6) motivated by the theoretical and experimental constraints. In Section 4 we discuss the production and decay of non-SM Higgses at the LHC, and then analyze in depth our different benchmark scenarios in Section 5, before concluding in Section 6.

*Here we take the assumption of a CP-conserving 2HDM. In the case of CP-violation, the three neutral Higgses are mixed together to form three mass eigenstates without definite CP properties.

†*e.g.* it has been shown in [18] that sizable mass splittings between the 2HDM new scalars favour a strong EW phase transition that could lead to baryogenesis.

2 Two Higgs Doublet Models: A Review

2.1 2HDM Lagrangian and Higgs Potential

In the 2HDM, we introduce two $SU(2)_L$ doublets Φ_i ($i = 1, 2$):

$$\Phi_i = \begin{pmatrix} \phi_i^+ \\ (v_i + \phi_i^0 + i\varphi_i)/\sqrt{2} \end{pmatrix}, \quad (2.1)$$

where v_i are the vacuum expectation values (vev) of the neutral components, satisfying $v_1^2 + v_2^2 = v^2$, with $v = 246$ GeV. The ratio of vevs is defined as $\tan \beta \equiv v_2/v_1$. The 2HDM Lagrangian for Φ_i can be written as

$$\mathcal{L} = \sum_i |D_\mu \Phi_i|^2 - V(\Phi_1, \Phi_2) + \mathcal{L}_{\text{Yuk}}, \quad (2.2)$$

where the first term denotes the kinetic term for the two Higgs doublets, $V(\Phi_1, \Phi_2)$ is the Higgs potential and the last term denotes the Yukawa interactions between Φ_i and the SM fermions. Assuming CP conservation and a soft \mathbb{Z}_2 symmetry breaking, the 2HDM Higgs potential can be written down as[†]:

$$\begin{aligned} V(\Phi_1, \Phi_2) = & m_{11}^2 \Phi_1^\dagger \Phi_1 + m_{22}^2 \Phi_2^\dagger \Phi_2 - m_{12}^2 (\Phi_1^\dagger \Phi_2 + \text{h.c.}) + \frac{\lambda_1}{2} (\Phi_1^\dagger \Phi_1)^2 + \frac{\lambda_2}{2} (\Phi_2^\dagger \Phi_2)^2 \\ & + \lambda_3 (\Phi_1^\dagger \Phi_1)(\Phi_2^\dagger \Phi_2) + \lambda_4 (\Phi_1^\dagger \Phi_2)(\Phi_2^\dagger \Phi_1) + \frac{1}{2} \left[\lambda_5 (\Phi_1^\dagger \Phi_2)^2 + \text{h.c.} \right]. \end{aligned} \quad (2.3)$$

After EW symmetry breaking, the physical 2HDM scalar spectrum consists of five states: two CP-even Higgses h, H with $m_h < m_H$, a CP-odd scalar A and a charged scalar pair H^\pm [24], which may be written as

$$\begin{aligned} \begin{pmatrix} H \\ h \end{pmatrix} &= \begin{pmatrix} c_\alpha & s_\alpha \\ -s_\alpha & c_\alpha \end{pmatrix} \begin{pmatrix} \phi_1^0 \\ \phi_2^0 \end{pmatrix}, \\ \begin{pmatrix} G \\ A \end{pmatrix} &= \begin{pmatrix} c_\beta & s_\beta \\ -s_\beta & c_\beta \end{pmatrix} \begin{pmatrix} \varphi_1 \\ \varphi_2 \end{pmatrix}, \quad \begin{pmatrix} G^\pm \\ H^\pm \end{pmatrix} = \begin{pmatrix} c_\beta & s_\beta \\ -s_\beta & c_\beta \end{pmatrix} \begin{pmatrix} \phi_1^\pm \\ \phi_2^\pm \end{pmatrix}, \end{aligned} \quad (2.4)$$

with the angle α parametrizing the mixing between the neutral CP-even components (we use the shorthand notation $s_x \equiv \sin x$, $c_x \equiv \cos x$, $t_x \equiv \tan x$). The Goldstone bosons G and G^\pm are absorbed as longitudinal components of the Z and W^\pm bosons. In the limit $c_{\beta-\alpha} = 0$ (the *alignment limit* for h), the state h can be identified with the SM Higgs, its couplings to fermions and gauge bosons being precisely those predicted by the SM[§]. It is thus convenient to describe the model in terms of t_β , $c_{\beta-\alpha}$, the physical scalar masses

[†]The most general scalar potential also contains the terms $[\lambda_6(\Phi_1^\dagger \Phi_1) + \lambda_7(\Phi_2^\dagger \Phi_2)](\Phi_1^\dagger \Phi_2) + \text{h.c.}$ (leading to potentially dangerous flavour changing neutral currents), which can however be forbidden by imposing a \mathbb{Z}_2 symmetry, softly broken by the m_{12}^2 term.

[§]We note that if the heavier neutral CP even Higgs H is identified with the observed 125 GeV SM-like Higgs, the alignment limit is instead described by $s_{\beta-\alpha} = 0$ [25].

m_h, m_H, m_A, m_{H^\pm} , the soft \mathbb{Z}_2 symmetry breaking parameter m_{12}^2 and the vev v . The quartic couplings in Eq. (2.3) can be expressed in terms of the physical masses and mixing angles as (see e.g. [26])

$$\begin{aligned} v^2 \lambda_1 &= \frac{m_H^2 c_\alpha^2 + m_h^2 s_\alpha^2 - m_{12}^2 t_\beta}{c_\beta^2}, & v^2 \lambda_2 &= \frac{m_H^2 s_\alpha^2 + m_h^2 c_\alpha^2 - m_{12}^2 t_\beta^{-1}}{s_\beta^2}, \\ v^2 \lambda_3 &= \frac{(m_H^2 - m_h^2) s_\alpha c_\alpha + 2m_{H^\pm}^2 s_\beta c_\beta - m_{12}^2}{s_\beta c_\beta}, & v^2 \lambda_4 &= \frac{(m_A^2 - 2m_{H^\pm}^2) s_\beta c_\beta + m_{12}^2}{s_\beta c_\beta}, \\ v^2 \lambda_5 &= \frac{-m_A^2 s_\beta c_\beta + m_{12}^2}{s_\beta c_\beta}. \end{aligned} \quad (2.5)$$

2.2 Interactions in the 2HDM

The couplings of the CP-even scalars to a pair of gauge bosons, arising from the Higgs kinetic term in Eq. (2.2), are [24]

$$g_{hZZ} = \frac{2im_Z^2}{v} s_{\beta-\alpha}, \quad g_{HZZ} = \frac{2im_Z^2}{v} c_{\beta-\alpha}, \quad g_{hWW} = \frac{2im_W^2}{v} s_{\beta-\alpha}, \quad g_{HWW} = \frac{2im_W^2}{v} c_{\beta-\alpha}. \quad (2.6)$$

The CP-odd scalar A does not couple to pairs of vector bosons, while the charged scalar H^\pm only couples to pair of vector bosons at loop level. In addition, the couplings of two scalars and one vector boson read

$$\begin{aligned} g_{hAZ} &= \frac{m_Z}{v} c_{\beta-\alpha} (p_A^\mu - p_h^\mu), & g_{HAZ} &= -\frac{m_Z}{v} s_{\beta-\alpha} (p_A^\mu - p_h^\mu), \\ g_{hH^\pm W^\mp} &= \pm \frac{im_W}{v} c_{\beta-\alpha} (p_{H^\pm}^\mu - p_h^\mu), & g_{HH^\pm W^\mp} &= \mp \frac{im_W}{v} s_{\beta-\alpha} (p_{H^\pm}^\mu - p_h^\mu), \\ g_{AH^\pm W^\mp} &= \frac{m_W}{v} (p_{H^\pm}^\mu - p_A^\mu), \end{aligned} \quad (2.7)$$

in which p^μ are the outgoing momentum for the corresponding particle. The hHZ -coupling is absent due to CP conservation. We note that, considering h (H) to be the SM-like 125 GeV Higgs with $c_{\beta-\alpha} = 0$ ($s_{\beta-\alpha} = 0$), gauge boson couplings to two non-SM like Higgses are unsuppressed, while the gauge boson couplings to h (H) and one non-SM like Higgs are suppressed by $c_{\beta-\alpha}$ ($s_{\beta-\alpha}$).

Regarding the cubic couplings among scalars arising from the 2HDM scalar potential Eq. (2.3), the relevant ones for our analysis are

$$\begin{aligned} g_{Hhh} &= -\frac{1}{4s_{2\beta}v} \left(\frac{4m_{12}^2}{s_\beta c_\beta} (c_{\beta-\alpha}^2 s_{\beta+\alpha} - 2s_{\beta-\alpha} c_{\beta-\alpha} c_{\beta+\alpha}) - (2m_h^2 + m_H^2) (s_{3\alpha-\beta} + s_{\alpha+\beta}) \right), \\ g_{HAA} &= -\frac{1}{4s_{2\beta}v} \left(\frac{4m_{12}^2}{s_\beta c_\beta} s_{\beta+\alpha} - 8m_A^2 c_{\beta-\alpha} s_\beta c_\beta - m_H^2 (s_{\alpha-3\beta} + 3s_{\alpha+\beta}) \right), \\ g_{HH^+H^-} &= -\frac{1}{4s_{2\beta}v} \left(\frac{4m_{12}^2}{s_\beta c_\beta} s_{\beta+\alpha} - 8m_{H^\pm}^2 c_{\beta-\alpha} s_\beta c_\beta - m_H^2 (s_{\alpha-3\beta} + 3s_{\alpha+\beta}) \right), \end{aligned} \quad (2.8)$$

which could mediate decays with H being the parent scalar: $H \rightarrow hh$, $H \rightarrow AA$ and $H \rightarrow H^+H^-$. As seen directly from Eq. (2.8), these couplings depend not only on the

mass spectrum, but also on the soft \mathbb{Z}_2 symmetry breaking term m_{12}^2 (we note here that the couplings shown in [24] assume the MSSM relation $m_{12}^2 = m_A^2 s_\beta c_\beta$). We also stress that for a light CP-odd scalar A with $m_A < m_h/2$, the decay channel $h \rightarrow AA$ could be open, being however very constrained experimentally[¶] (see [28] for a discussion of this region of the 2HDM parameter space).

| State | Up-type fermions | Down-type fermions |
|-------|--|---|
| h | $c_\alpha/s_\beta = s_{\beta-\alpha} + c_{\beta-\alpha}/t_\beta$ | $-s_\alpha/c_\beta = s_{\beta-\alpha} - c_{\beta-\alpha} t_\beta$ |
| H | $s_\alpha/s_\beta = c_{\beta-\alpha} - s_{\beta-\alpha}/t_\beta$ | $c_\alpha/c_\beta = c_{\beta-\alpha} + s_{\beta-\alpha} t_\beta$ |
| A | $1/t_\beta$ | t_β |

Table 1. Tree-level couplings to up-type fermions and down-type fermions normalized to their SM values for h , H and A in the Type II 2HDM.

Finally, as is well-known the couplings of the 2HDM scalars to SM fermions, contained in \mathcal{L}_{Yuk} in Eq. (2.2) are not univocally determined by the gauge structure of the model. In the presence of a \mathbb{Z}_2 symmetry guaranteeing the absence of tree-level flavour changing neutral currents [29], four possible 2HDM types exist (see [30] for a discussion). The couplings of the neutral scalar states to SM fermions, normalized to their SM values, can be expressed in terms of functions of α and β , shown in Table 1 for the particular case of a Type II 2HDM (one Higgs doublet Φ_2 couples to the up-type quarks, while the other Higgs doublet Φ_1 couples to the down-type quarks and leptons).

2.3 The Alignment Limit and the Role of m_{12}^2

It is useful to cast the relations between the quartic couplings and the physical masses Eq. (2.5) in terms of $c_{\beta-\alpha}$, which characterizes the departure from the alignment limit for h

$$\begin{aligned}
v^2 \lambda_1 &= m_h^2 - \frac{t_\beta (m_{12}^2 - m_H^2 s_\beta c_\beta)}{c_\beta^2} + (m_h^2 - m_H^2) [c_{\beta-\alpha}^2 (t_\beta^2 - 1) - 2t_\beta s_{\beta-\alpha} c_{\beta-\alpha}], \\
v^2 \lambda_2 &= m_h^2 - \frac{(m_{12}^2 - m_H^2 s_\beta c_\beta)}{t_\beta s_\beta^2} + (m_h^2 - m_H^2) [c_{\beta-\alpha}^2 (t_\beta^{-2} - 1) + 2t_\beta^{-1} s_{\beta-\alpha} c_{\beta-\alpha}], \\
v^2 \lambda_3 &= m_h^2 + 2m_{H^\pm}^2 - 2m_H^2 - \frac{(m_{12}^2 - m_H^2 s_\beta c_\beta)}{s_\beta c_\beta} - (m_h^2 - m_H^2) [2c_{\beta-\alpha}^2 + s_{\beta-\alpha} c_{\beta-\alpha} (t_\beta - t_\beta^{-1})], \\
v^2 \lambda_4 &= m_A^2 - 2m_{H^\pm}^2 + m_H^2 + \frac{(m_{12}^2 - m_H^2 s_\beta c_\beta)}{s_\beta c_\beta}, \\
v^2 \lambda_5 &= m_H^2 - m_A^2 + \frac{(m_{12}^2 - m_H^2 s_\beta c_\beta)}{s_\beta c_\beta}. \tag{2.9}
\end{aligned}$$

Current data from LHC Run 1 favour the alignment limit $c_{\beta-\alpha} = 0$ [31] (see also [6–8, 10–12, 14]). For a Type II 2HDM the only other allowed possibility is the *wrong-sign*

[¶]The possibility of a light charged scalar with $m_{H^\pm} < m_h/2$ has been ruled out experimentally by LEP, which puts a lower bound $m_{H^\pm} > 80$ GeV for Type II ($m_{H^\pm} > 72$ GeV for Type I) 2HDM [27], thus forbidding the decay $h \rightarrow H^+ H^-$.

scenario [32] $s_{\beta+\alpha} \simeq 1$ (compatible with measurements of Higgs signal strengths for $t_\beta > 3$). For $c_{\beta-\alpha} = 0$, the relations Eq. (2.9) simply become

$$\begin{aligned}
v^2 \lambda_1 &= m_h^2 - \frac{t_\beta (m_{12}^2 - m_H^2 s_\beta c_\beta)}{c_\beta^2}, \\
v^2 \lambda_2 &= m_h^2 - \frac{(m_{12}^2 - m_H^2 s_\beta c_\beta)}{t_\beta s_\beta^2}, \\
v^2 \lambda_3 &= m_h^2 + 2m_{H^\pm}^2 - 2m_H^2 - \frac{(m_{12}^2 - m_H^2 s_\beta c_\beta)}{s_\beta c_\beta}, \\
v^2 \lambda_4 &= m_A^2 - 2m_{H^\pm}^2 + m_H^2 + \frac{(m_{12}^2 - m_H^2 s_\beta c_\beta)}{s_\beta c_\beta}, \\
v^2 \lambda_5 &= m_H^2 - m_A^2 + \frac{(m_{12}^2 - m_H^2 s_\beta c_\beta)}{s_\beta c_\beta}.
\end{aligned} \tag{2.10}$$

The combination $m_{12}^2 - m_H^2 s_\beta c_\beta$ in Eq. (2.10) will play a key role in the following discussion: the value of m_{12}^2 is not fixed by the mass spectrum or the scalar couplings to gauge bosons and fermions, only entering the trilinear scalar couplings Eq. (2.8). Its possible allowed values are dictated by theoretical constraints on the 2HDM parameter space, namely the boundedness from below of the scalar potential Eq. (2.3) and the stability of the EW minimum, and the requirements of perturbativity and tree-level unitarity on the quartic couplings λ_i , as shown in the next section. These have a large impact on the allowed values of masses m_H , m_A , m_{H^\pm} , m_{12}^2 and t_β (and $c_{\beta-\alpha}$ away from alignment), as the absence of a value of m_{12}^2 satisfying the theoretical constraints for a given set of values for m_H , m_A , m_{H^\pm} and t_β , indicates that such set of values is not physically viable (see e.g. [15]).

3 2HDM Theoretical and Experimental Constraints

3.1 Vacuum Stability

In order to have a stable vacuum, the following conditions need to be fulfilled [26]

$$\lambda_1 > 0, \quad \lambda_2 > 0, \quad \lambda_3 > -\sqrt{\lambda_1 \lambda_2}, \quad \lambda_3 + \lambda_4 - |\lambda_5| > -\sqrt{\lambda_1 \lambda_2}. \tag{3.1}$$

For $c_{\beta-\alpha} = 0$, satisfying the first two conditions requires $m_{12}^2 - m_H^2 s_\beta c_\beta \lesssim 0$ for either $t_\beta > 1$ or $t_\beta < 1$, as seen from Eq. (2.10). Moreover, Eq. (2.9) shows that a departure from alignment generically has a negative impact on the first two stability conditions. Focusing on the alignment limit, the first two requirements are automatically satisfied for $m_{12}^2 - m_H^2 s_\beta c_\beta = 0$, with the last two given by

$$m_h^2 + m_{H^\pm}^2 - m_H^2 > 0, \quad m_h^2 + m_A^2 - m_H^2 > 0. \tag{3.2}$$

This implies that for $m_H > m_A, m_{H^\pm}$, the mass splittings between the heavy CP-even Higgs H and the other heavy scalars A and H^\pm have to be small, such that the decays of H into AZ , AA , H^+H^- or $H^\pm W^\mp$ are not kinematically allowed. For $m_{12}^2 = 0$ all four stability conditions of Eq. (3.1) are automatically fulfilled. The allowed region in

the m_{12} vs. t_β plane is shown in the left panel of Figure 1 for $m_A = m_{H^\pm} = 400$ GeV and $m_H = 200, 300, 400$ GeV as an illustration. As seen from Figure 1, the regions $m_{12}^2 < m_H^2 s_\beta c_\beta$ are generically allowed by the vacuum stability requirement.

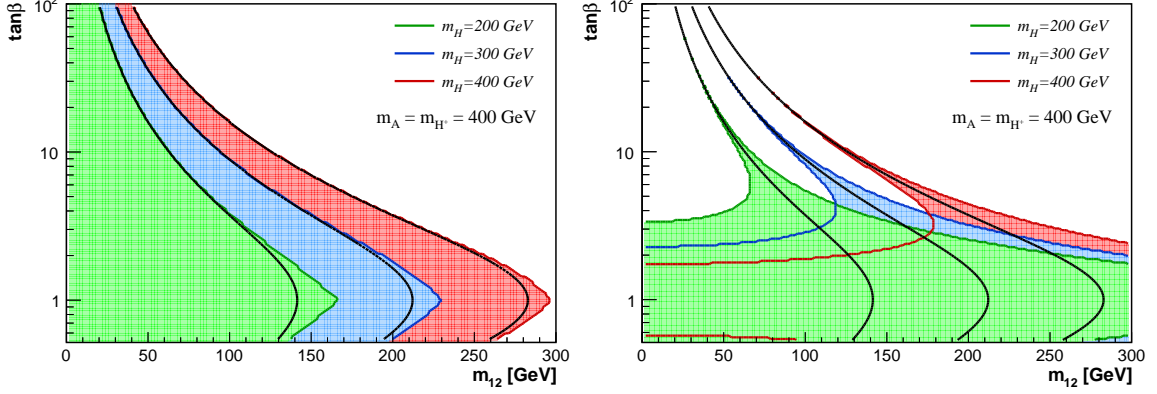


Figure 1. Allowed region in the (m_{12}, t_β) plane from vacuum stability (left panel) and unitarity $|\Lambda_i| < 8\pi$ (right panel) for $m_H = 400$ GeV (red), 300 GeV (blue) and 200 GeV (green), assuming $c_{\beta-\alpha} = 0$ and $m_A = m_{H^\pm} = 400$ GeV. The black lines denote the relation $m_{12}^2 = m_H^2 s_\beta c_\beta$.

3.2 Perturbativity and Unitarity

Upon imposing the perturbativity condition $|\lambda_i| \leq 4\pi$, the strongest constraints in the alignment limit come respectively from $v^2 \lambda_1 \sim t_\beta^3 (m_{12}^2 - m_H^2 s_\beta c_\beta)$ for $t_\beta \gg 1$ and $v^2 \lambda_2 \sim t_\beta^{-3} (m_{12}^2 - m_H^2 s_\beta c_\beta)$ for $t_\beta \ll 1$. Thus, perturbativity requires $|m_{12}^2 - m_H^2 s_\beta c_\beta| \lesssim v^2$ unless $t_\beta \sim 1$. Moreover, even for $m_{12}^2 = m_H^2 s_\beta c_\beta$, perturbativity of λ_{3-5} imposes constraints on the size of the mass splittings among the new scalars.

Even stronger constraints are found when requiring tree-level unitarity^{||} of the scattering matrix in the 2HDM scalar sector [33]. The eigenvalues of the scattering matrix read

$$\begin{aligned}
 \Lambda_{1,2} &= \lambda_3 \pm \lambda_4, \\
 \Lambda_{3,4} &= \lambda_3 \pm \lambda_5, \\
 \Lambda_{5,6} &= \lambda_3 + 2\lambda_4 \pm 3\lambda_5, \\
 \Lambda_{7,8} &= \frac{1}{2} \left(\lambda_1 + \lambda_2 \pm \sqrt{(\lambda_1 - \lambda_2)^2 + 4\lambda_4^2} \right), \\
 \Lambda_{9,10} &= \frac{1}{2} \left(\lambda_1 + \lambda_2 \pm \sqrt{(\lambda_1 - \lambda_2)^2 + 4|\lambda_5|^2} \right), \\
 \Lambda_{11,12} &= \frac{1}{2} \left(3(\lambda_1 + \lambda_2) \pm \sqrt{9(\lambda_1 - \lambda_2)^2 + 4(2\lambda_3 + \lambda_4)^2} \right). \tag{3.3}
 \end{aligned}$$

Performing a partial-wave expansion of the scattering amplitudes yields limits on the partial wave amplitudes, which for the $J = 0$ case translate into the constraint $|\text{Re}(\Lambda_i)| < 8\pi$ (see *e.g.* [34]), which we consider here. A quick inspection of Eq. (3.3) shows that for $t_\beta \gg 1$ the scattering matrix eigenvalues scale as $\Lambda_{7,9,11} \sim \lambda_1$ (particularly $\Lambda_{11} \simeq 3\lambda_1$), which

^{||}An analysis of unitarity constraints at one-loop level has been performed in [34].

again imposes $|m_{12}^2 - m_H^2 s_\beta c_\beta| \lesssim v^2$ (and yields an even stronger constraint than the perturbativity one). A similar argument follows for $t_\beta \ll 1$, this time with $\Lambda_{7,9,11} \sim \lambda_2$. As a result, $m_{12}^2 \approx m_H^2 s_\beta c_\beta$ is strongly preferred unless $t_\beta \sim 1$, as shown explicitly in the right panel of Figure 1 (for $m_A = m_{H^\pm}$). In the limit $m_{12}^2 = m_H^2 s_\beta c_\beta$, the scattering matrix eigenvalues from Eq. (3.3) become independent of t_β (in alignment $c_{\beta-\alpha} = 0$) and read

$$\begin{aligned} \Lambda_{1(9),10} v^2 &= m_h^2 \mp m_H^2 \pm m_A^2, & \Lambda_2 v^2 &= m_h^2 - 3m_H^2 - m_A^2 + 4m_{H^\pm}^2, \\ \Lambda_3 v^2 &= m_h^2 - m_H^2 - m_A^2 + 2m_{H^\pm}^2, & \Lambda_{4,5} v^2 &= m_h^2 \mp 3m_H^2 \pm m_A^2 \pm 2m_{H^\pm}^2, \\ \Lambda_6 v^2 &= m_h^2 - 3m_H^2 + 5m_A^2 - 2m_{H^\pm}^2, & \Lambda_{7,8} v^2 &= m_h^2 \pm m_H^2 \pm m_A^2 \mp 2m_{H^\pm}^2, \\ \Lambda_{11} v^2 &= 5m_h^2 - 3m_H^2 + m_A^2 + 2m_{H^\pm}^2, & \Lambda_{12} v^2 &= m_h^2 + 3m_H^2 - m_A^2 - 2m_{H^\pm}^2, \end{aligned} \quad (3.4)$$

such that $|\Lambda_i| < 8\pi$ (note that Λ_i are real) impose upper limits on the mass splittings (although not on the masses themselves). We also note that for $m_{12}^2 = 0$, Λ_{1-6} are independent of t_β (depending only on the scalar masses) while Λ_{7-12} do depend on t_β , which once again results in $t_\beta \approx 1$ being the only accessible region for large mass splittings in this case.

3.3 Electroweak Precision Measurements

Measurements of EW precision observables (EWPO) impose strong constraints on the 2HDM mass spectrum. Adopting the current 95% C.L. constraints on the S and T oblique parameters (with $U = 0$) [35], the allowed region of parameter space in the (m_A, m_{H^\pm}) plane is shown, for $c_{\beta-\alpha} = 0$ (neither t_β nor m_{12}^2 affect S and T), in the left panel of Figure 2 respectively for $m_H = 400$ GeV (red), $m_H = 300$ GeV (blue) and $m_H = 200$ GeV (green). Satisfying EWPO constraints requires the charged scalar mass to be close to one of the heavy neutral scalar masses: $m_{H^\pm} \approx m_H$ or $m_{H^\pm} \approx m_A$.

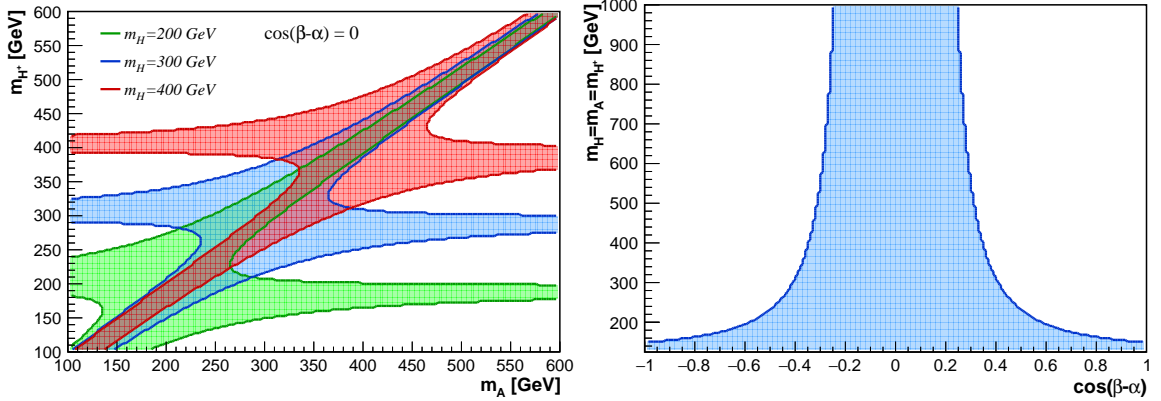


Figure 2. Left: 2HDM parameter space in the (m_A, m_{H^\pm}) plane allowed at 95% C.L. by S and T measurements [35], for $m_H = 400$ GeV (red), $m_H = 300$ GeV (blue) and $m_H = 200$ GeV (green), assuming $c_{\beta-\alpha} = 0$. Right: $S - T$ constraints in the $(c_{\beta-\alpha}, m_H)$ plane for $m_H = m_A = m_{H^\pm}$.

Away from the alignment limit, additional contributions to S and T proportional to $c_{\beta-\alpha}$ appear [24] (see also [36]), such that the scenario $m_H = m_A = m_{H^\pm}$ is only allowed for small $|c_{\beta-\alpha}|$ once $m_H \gg v$ is realized, as shown in the right panel of Figure 2. The departure from alignment also allows for mild mass splittings among all the new scalars

(e.g. $m_A > m_H + m_Z$ and $m_H \gtrsim m_{H^\pm} + m_W$), which however does not significantly alter the phenomenology of exotic Higgs decays at the LHC, discussed in detail in Section 5.

3.4 Flavour Constraints

Various flavour measurements [37] provide indirect constraints on the charged scalar mass m_{H^\pm} as a function of t_β . The different limits are computed for the case of a Type II 2HDM with SUPERISO [38, 39], and shown in the left panel of Figure 3. The most stringent of these** comes from the measurement of the branching fraction (BR) of $b \rightarrow s\gamma$ ($B_d^0 \rightarrow X_s\gamma$), which sets a limit $m_{H^\pm} > 480$ GeV at 95 % C.L. [43] (we note that the limit is even stronger for $t_\beta < 2$). For large $t_\beta \gtrsim 20$, the lower limit on m_{H^\pm} set by the measurement of the branching fraction $B_d^+ \rightarrow \tau^+\nu$ is significantly stronger, with $m_{H^\pm} \gtrsim 700$ GeV for $t_\beta = 30$. Similarly, the region $t_\beta \lesssim 1$ is very strongly constrained by $B_s^0 \rightarrow \mu\mu$ and Δm_{B_d} .

For $m_H = 125$ GeV and $s_{\beta-\alpha} = 0$, when the heavy CP-even scalar H is the SM-like Higgs, the mass of the light CP-even Higgs h is constrained by flavour measurements as well, as shown in the right panel of Figure 3 for Type II 2HDM. The strongest constraint in this case comes from $B_s^0 \rightarrow \mu^+\mu^-$, which can exclude up to $m_h < 100$ GeV (the precise bound depending on m_{12}^2 and t_β) for masses m_{H^\pm} satisfying the $b \rightarrow s\gamma$ constraint.

Note that flavour constraints are typically very model dependent. Contributions from additional sectors in the model could relax the constraints, as has e.g. been studied in the MSSM framework for $b \rightarrow s\gamma$ [44]. Being mostly focused on the collider aspects of 2HDM Higgses, we will not consider flavour as a hard constraint in the following, however indicating its effect on the parameter space under consideration.

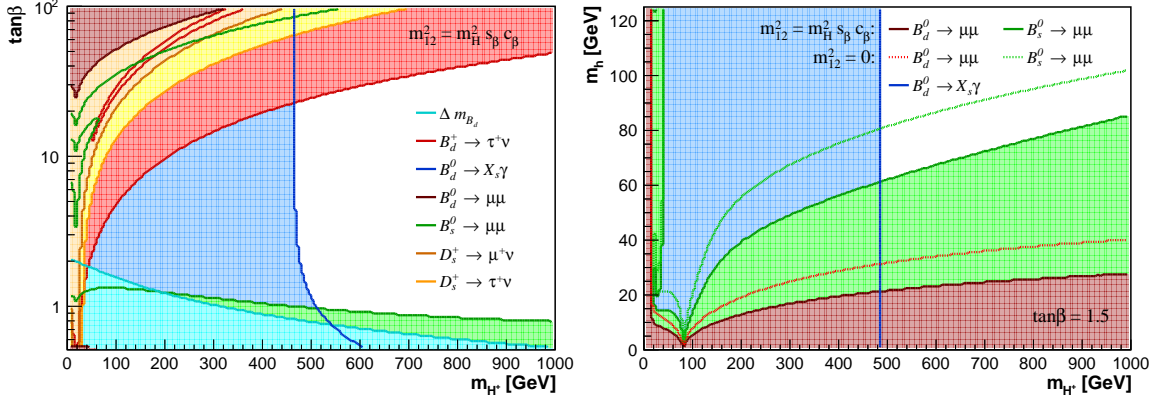


Figure 3. Type II 2HDM parameter space excluded by flavour constraints (see text for details).

3.5 LHC and LEP Constraints

We now review the constraints from direct searches of the new scalars. Besides the LEP bound $m_{H^\pm} > 80$ GeV (72 GeV) for Type II (I) 2HDM [27], LEP searches for $e^+e^- \rightarrow$

**We note here that the recent measurement from the BaBar Collaboration of the ratios of $B \rightarrow D^*\tau\nu$ to $B \rightarrow D^*\ell\nu$ decays and $B \rightarrow D\tau\nu$ to $B \rightarrow D\ell\nu$ decays cannot be accommodated within the Type II 2HDM [40]. However, a new measurement of the former ratio by the Belle Collaboration [41, 42] is in tension with this conclusion. Since this matter is not settled yet, we choose not to include these flavour measurements in our discussion.

AH ($H \rightarrow bb/\tau\tau$, $A \rightarrow bb/\tau\tau$) constrain the sum of the masses $m_A + m_H \gtrsim 209$ GeV [45]. At the LHC, the searches for A/H in bb -associated production and decaying to $\tau\tau$ by ATLAS/CMS [46, 47] constrain the high t_β region in the Type II 2HDM. Away from alignment, searches by ATLAS/CMS for $H \rightarrow W^+W^-$, ZZ [48–50], $A \rightarrow hZ$ ($h \rightarrow bb$) [51, 52] and $H \rightarrow hh \rightarrow bb\gamma\gamma, bbbb$ [53–55] yield strong constraints on the $(c_{\beta-\alpha}, t_\beta)$ plane as a function of the respective mass m_H/m_A (see e.g. [13, 15]). We however stress that the limits summarized above can be significantly weakened once exotic Higgs decay channels are open [15–17, 19, 21]). Searches for these new channels, e.g. via $A/H \rightarrow HZ/AZ$ are then crucial for probing 2HDM scenarios with large mass splittings among the new states (i.e. hierarchical 2HDM scenarios), and there is already ongoing effort by CMS in this direction [22, 23].

Finally, ATLAS/CMS searches impose constraints on the charged scalar [56, 57] beyond those of LEP. A light charged scalar $m_{H^\pm} \lesssim m_t$ is mostly excluded by the non-observation of the decay $t \rightarrow H^+b \rightarrow \tau\nu b$ where the top is produced in top pair production. For $m_{H^\pm} > m_t$, the current limit is very weak and only constrains the high t_β region for m_{H^\pm} not much above the top mass (see [19] for a detailed discussion).

3.6 From Constraints to 2HDM Benchmarks

The combination of previous constraints provides a key guideline to the design of simplified 2HDM benchmark scenarios for LHC Run 2 searches at 13 TeV. EWPO measurements require the mass of the charged scalar to be close to the mass of one of the neutral scalars, and so we fix $m_{H^\pm} = m_H$ or $m_{H^\pm} = m_A$ in the following. In addition, measurements of Higgs signal strengths at the LHC favour the alignment limit ($c_{\beta-\alpha} = 0$ if h is the 125 GeV SM-like Higgs), particularly for Type II 2HDM. We then focus our analysis mostly on the alignment limit, and only consider deviations from alignment when discussing possible decays of the new scalars into the SM-like Higgs h .

Regarding the impact of theoretical constraints on the 2HDM parameter space, the previous discussion shows that satisfying unitarity/perturbativity and vacuum stability bounds (close to the alignment limit) for arbitrary values of t_β requires $m_{12}^2 = m_H^2 s_\beta c_\beta$ and $m_H \lesssim m_A, m_{H^\pm}$. Alternatively, stability is satisfied for any mass ordering if $m_{12}^2 = 0$, while unitarity requires in this case a low value of t_β . We thus consider these two scenarios as benchmark cases for our analysis:

- **Case 1:** $m_{12}^2 = m_H^2 s_\beta c_\beta$ ^{††}
 - From Eq. (3.2), vacuum stability requires $m_H \lesssim m_A$ and $m_H \lesssim m_{H^\pm}$, and thus the exotic decays $H \rightarrow AZ$ and $H \rightarrow H^\pm W^\mp$ are not kinematically allowed.
 - Unitarity requires $|\Lambda_i| < 8\pi$, constraining the mass differences among the new scalar states (but not the absolute mass values). In particular, using Eq. (3.4) we obtain the bound $|5(m_A^2 - m_H^2) + m_h^2| < 8\pi v^2$ if $m_{H^\pm} = m_H$, and the bound $|3(m_A^2 - m_H^2) + 5m_h^2| < 8\pi v^2$ if $m_{H^\pm} = m_A$.

^{††}The authors of [58] have shown that this case is preferred when requiring the 2HDM to be stable up to the Planck scale.

- The cubic scalar couplings Eq. (2.8) now read

$$\begin{aligned}
g_{Hhh} &= -\frac{c_{\beta-\alpha}}{s_{2\beta}v} [2(m_H^2 + m_h^2) s_{2\alpha} - m_H^2 s_{2\beta}] \\
g_{HAA} &= -\frac{c_{\beta-\alpha}}{2v} (m_H^2 - 2m_A^2) \\
g_{HH^+H^-} &= -\frac{c_{\beta-\alpha}}{2v} (m_H^2 - 2m_{H^\pm}^2)
\end{aligned} \tag{3.5}$$

In the alignment limit $c_{\beta-\alpha} = 0$ all these couplings vanish, and therefore the decays $H \rightarrow AA$, $H \rightarrow H^+H^-$ and $H \rightarrow hh$ are absent ($H \rightarrow AA$ and $H \rightarrow H^+H^-$ are also not kinematically allowed for $m_{12}^2 = m_H^2 s_\beta c_\beta$).

• **Case 2:** $m_{12}^2 = 0$ and $t_\beta \sim 1$ ^{††}

- Vacuum stability does not constrain the parameter space. In particular $m_H > m_A$, m_{H^\pm} is now possible, allowing the decays $H \rightarrow AZ$ and $H \rightarrow H^\pm W^\mp$ (and potentially also $H \rightarrow AA$ and $H \rightarrow H^+H^-$).
- Unitarity imposes an upper bound on the scalar masses (not only on the mass splittings). This bound scales as t_β^{-2} for $t_\beta > 1$ and as t_β^2 for $t_\beta < 1$, such that only the region $t_\beta \sim 1$ is allowed (we recall that in Type II 2HDM, at least one of the neutral scalars needs to be heavy due to the combination of EWPO and flavour constraints).
- The cubic scalar couplings Eq. (2.8) now read

$$\begin{aligned}
g_{Hhh} &= \frac{c_{\beta-\alpha}}{2s_{2\beta}v} (2m_h^2 + m_H^2) [(c_{\beta-\alpha}^2 - s_{\beta-\alpha}^2) s_{2\beta} - 2s_{\beta-\alpha} c_{\beta-\alpha} c_{2\beta}] \\
g_{HAA} &= -\frac{1}{2s_{2\beta}v} [(m_H^2 - 2m_A^2) c_{\beta-\alpha} s_{2\beta} + 2m_H^2 s_{\beta-\alpha} c_{2\beta}] \\
g_{HH^+H^-} &= -\frac{1}{2s_{2\beta}v} [(m_H^2 - 2m_{H^\pm}^2) c_{\beta-\alpha} s_{2\beta} + 2m_H^2 s_{\beta-\alpha} c_{2\beta}]
\end{aligned} \tag{3.6}$$

In the alignment limit the coupling g_{Hhh} vanishes and thus the decay $H \rightarrow hh$ is absent. However, the couplings g_{HAA} and $g_{HH^+H^-}$ are non-vanishing as long as $t_\beta \neq 1$.

For our analysis of benchmark scenarios away from alignment, which focus on the decays of A , H , H^\pm into the SM-like Higgs h , we consider the same two cases above for consistency (even though these cases are motivated by theoretical constraints for $c_{\beta-\alpha} = 0$).

4 LHC Production and Decay of 2HDM Higgses

We now discuss the salient features of the production and decay of the new 2HDM scalars at the LHC. The production of the CP-even and CP-odd neutral scalars H , A at the 13 TeV LHC occurs via gluon fusion ($gg \rightarrow H/A$) and bb -associated production. Gluon

^{††}This case has also been analyzed in [59].

fusion is the dominant production mechanism for small and moderate values of t_β , while for Type II 2HDM, bb -associated production dominates at large t_β . In both cases, we compute the production cross section for H and A at NNLO in QCD via SusHi [60] (for H , the cross section does depend on $c_{\beta-\alpha}$, and in that case we consider the alignment limit $c_{\beta-\alpha} = 0$). For the charged scalar H^\pm , the dominant production mode for $m_{H^\pm} > m_t$ is in association with a tb pair, and we use the NLO cross section values provided by the Higgs Cross Section Working Group (HXS WG) for $m_{H^\pm} > 200$ GeV [61]. A light charged scalar ($m_{H^\pm} < m_t$) is mainly produced through top quark decays $t \rightarrow H^\pm b$, and we use TOP++2.0 [62] to compute the top pair production to NNLO in QCD, assuming a top-quark mass $m_t = 172.5$ GeV. The LHC production cross sections for H , A and H^\pm at 13 TeV are shown in Appendix A.

Regarding the decays of the new scalars, in the alignment limit $c_{\beta-\alpha} = 0$ the conventional (SM-like) decays of A and H are into tt (if kinematically accessible), bb , cc , $\tau\tau$, and with a highly suppressed branching fraction into gg , $\gamma\gamma$ and $\mu\mu$. When open, the decay into tt is dominant for low and moderate t_β , followed by the decay into bb . At high t_β , for Type II 2HDM, the decay into $\tau\tau$ becomes important, where the decay into bb can dominate even above the tt threshold. For the CP-even Higgs H , the decay into massive gauge bosons W^+W^- and ZZ is present away from the alignment limit, and dominates as soon as the departure from alignment is sizeable. For the charged scalar, the decay $H^\pm \rightarrow tb$ dominates once it is kinematically open, followed by $H^\pm \rightarrow \tau\nu$, cs and cb . In the following, we compute all 2HDM branching fractions using 2HDMC [63].

| Parent Scalar | Decay | Possible Final States | Channels in 2HDM |
|-------------------|---------------|---|--|
| Neutral H, A | $H_i H_i$ | $(bb/\tau\tau/WW/ZZ/\gamma\gamma) (bb/\tau\tau/WW/ZZ/\gamma\gamma)$ | $H \rightarrow AA, hh$ |
| | $H_i Z$ | $(bb/\tau\tau/WW/ZZ/\gamma\gamma) (\ell\ell/qq/\nu\nu)$ | $H \rightarrow AZ, A \rightarrow HZ, hZ$ |
| | $H^+ H^-$ | $(tb/\tau\nu/cs) (tb/\tau\nu/cs)$ | $H \rightarrow H^+ H^-$ |
| | $H^\pm W^\mp$ | $(tb/\tau\nu/cs) (\ell\nu/qq')$ | $H/A \rightarrow H^\pm W^\mp$ |
| Charged H^\pm | $H_i W^\pm$ | $(bb/\tau\tau/WW/ZZ/\gamma\gamma) (\ell\nu/qq')$ | $H^\pm \rightarrow hW^\pm, HW^\pm, AW^\pm$ |

Table 2. Summary of exotic decay modes for non-SM Higgs bosons. For each type of exotic decays (second column), we present possible final states (third column) and relevant channels in 2HDM (fourth column). In the second column, $H_i = h, H, A$.

We here stress that the above conventional decays of the new 2HDM scalars become suppressed once exotic (non SM-like) decay modes open up. These can be decays involving several states among H, A, H^\pm , in the presence of a large mass splitting among the new scalars (see e.g. [16–21] for existing studies on individual channels), and/or decays into the SM-like Higgs boson h , namely $H \rightarrow hh$, $A \rightarrow hZ$, $H^\pm \rightarrow hW^\pm$, which are possible for $c_{\beta-\alpha} \neq 0$ and are also considered in the following as exotic (despite involving SM decay products) as they don't occur in the SM. In the former case, we can further distinguish between the decay of a new scalar into another one and a gauge boson, and the potential decays of H into either AA or $H^+ H^-$. The different types of exotic decay modes for the 2HDM are summarized in Table 2.

The impact of the presence of exotic Higgs decay modes on the branching ratios is shown in Figure 4 for $c_{\beta-\alpha} = 0$. The top two panels show the relevant branching fractions

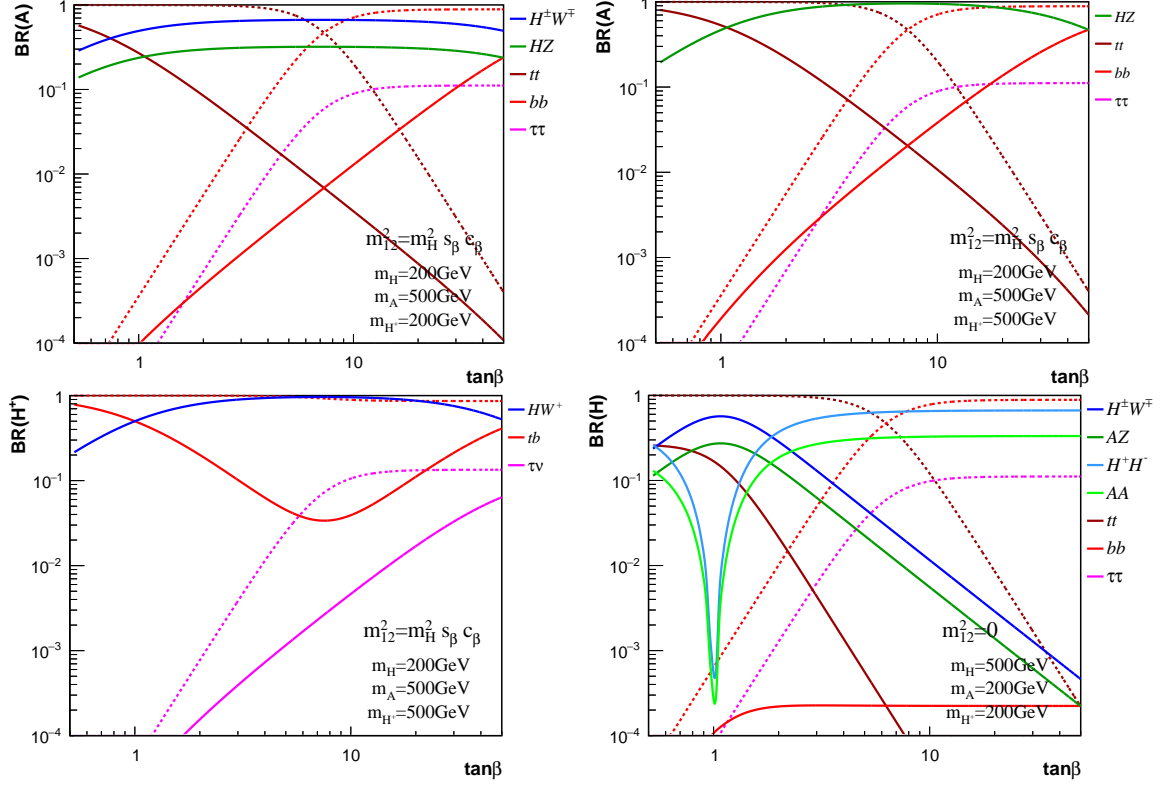


Figure 4. Branching fractions in Type II 2HDM as a function of t_β for $c_{\beta-\alpha} = 0$, with parent and daughter scalar masses fixed to 500 GeV and 200 GeV, respectively. Top: Branching fractions for A with $m_H = m_{H^\pm} < m_A$ (left) and with $m_H < m_A = m_{H^\pm}$ (right), in both cases for $m_{12}^2 = m_H^2 s_\beta c_\beta$. Bottom: Branching fractions for H^\pm with $m_H < m_{H^\pm} = m_A$ and $m_{12}^2 = m_H^2 s_\beta c_\beta$ (left) and for H with $m_H > m_{H^\pm} = m_A$ and $m_{12}^2 = 0$ (right). In all cases, dashed lines indicate the branching fractions to SM fermion pairs when exotic decay modes are absent.

of A with $m_H = m_{H^\pm} < m_A$ (left), and $m_H < m_A = m_{H^\pm}$ (right) for $m_A = 500$ GeV and $m_H = 200$ GeV, with $m_{12}^2 = m_H^2 s_\beta c_\beta$. In the former case, the decays $A \rightarrow H^\pm W^\mp$ (solid blue) and $A \rightarrow HZ$ (solid green) completely dominate over the SM decays $A \rightarrow tt, bb, \tau\tau$ for most values of t_β , with $\text{BR}(A \rightarrow H^\pm W^\mp) \sim 50\text{--}60\%$ and $\text{BR}(A \rightarrow HZ) \sim 20\text{--}30\%$, while in the latter with $A \rightarrow H^\pm W^\mp$ being absent, the branching fraction of $A \rightarrow HZ$ is more than 50%. Decays of $A \rightarrow tt, bb$ are only important for very small or very large t_β . The dashed lines show for comparison the branching fractions into the conventional SM states when the exotic decays are absent, which highlights the suppression the SM channels suffer in the presence of the exotic decays. The bottom left panel in Figure 4 shows the branching fractions of H^\pm for $m_H < m_{H^\pm} = m_A$ (with $m_A = 500$ GeV and $m_H = 200$ GeV) and $m_{12}^2 = m_H^2 s_\beta c_\beta$. The decay $H^\pm \rightarrow HW^\pm$ (solid blue) dominates with $\text{BR}(H^\pm \rightarrow HW^\pm) \gtrsim 50\%$, particularly for a not too heavy state H^\pm . In that case, $H^\pm \rightarrow tb$ is suppressed to be about few percent for intermediate t_β , and only reaches about 50% in the very small and very large t_β region. Finally, the bottom right panel in Figure 4 shows the branching fractions of H for $m_H > m_{H^\pm} = m_A$ (with $m_H = 500$ GeV

and $m_A = 200$ GeV) and $m_{12}^2 = 0$. In this case the decays $H \rightarrow AA$ and $H \rightarrow H^+H^-$ are allowed and dominate over most of the t_β region, except for $t_\beta \sim 1$, where $H \rightarrow AZ$ and $H \rightarrow H^\pm W^\mp$ become dominant due to the accidental suppression of the HH^+H^- and HAA couplings at $t_\beta \sim 1$. Note however that for $m_{12}^2 = 0$ the theoretical constraints do not allow a significant departure from $t_\beta \sim 1$, such that a large branching fraction for $H \rightarrow AZ$ and $H \rightarrow H^\pm W^\mp$ is expected. Decays to SM fermions are highly suppressed in this scenario.

5 2HDM Planes for Exotic Higgs Decays

Our analysis of exotic Higgs decays in the 2HDM focuses on a few key benchmark planes which show the complementarity among different LHC search channels for the new scalars. We first focus on the alignment limit: $c_{\beta-\alpha} = 0$ for $m_H > m_h = 125$ GeV and $s_{\beta-\alpha} = 0$ for $m_h < m_H = 125$ GeV. In this context, we consider two possible mass planes: m_A vs. $m_H = m_{H^\pm}$ (Plane I) and m_H vs. $m_A = m_{H^\pm}$ (Plane II). These two choices are motivated by EWPO constraints (recall the discussion in Section 3.3). This is in contrast to a potential m_{H^\pm} vs. $m_H = m_A$ plane, highly constrained by EWPO to a small mass splitting $m_{H^\pm} - m_{H/A}$ which closes the phase space needed for on-shell exotic Higgs decays^{§§}, so that we don't consider such benchmark plane in our current study. Finally let us remark that, while we do not impose the flavour bounds as hard constraints on our 2HDM benchmark planes (recall the discussion in Section 3.4), we do show them as indicative in the following. Our 2HDM benchmark plane (BP) scenarios in alignment are then:

Plane I: m_A vs. $m_H = m_{H^\pm}$

- BP IA: $m_A > m_H = m_{H^\pm}$.

As discussed in Section 3.6, this mass ordering is allowed for Case 1 ($m_{12}^2 = m_H^2 s_\beta c_\beta$ and all t_β values) and Case 2 ($m_{12}^2 = 0$ and $t_\beta \sim 1$). We thus consider four scenarios: Case 1 with $t_\beta = 1.5, 7, 30$ and Case 2 with $t_\beta = 1.5$.

- BP IB: $m_A < m_H = m_{H^\pm}$.

This mass ordering is not compatible with Case 1 due to vacuum stability (see Sections 3.1 and 3.6). Thus, we only consider Case 2 with $t_\beta = 1.5$ ^{¶¶}.

Plane II: m_H vs. $m_A = m_{H^\pm}$

- BP IIA: $m_H > m_A = m_{H^\pm}$.

As for BP IB, this mass ordering is not compatible with Case 1, and so we only consider Case 2 with $t_\beta = 1.5$.

^{§§}As discussed in Section 3.3, a sizable departure from alignment could allow for a mass hierarchy $m_A > m_H + m_Z$ (such that $A \rightarrow HZ$ is kinematically allowed) and $m_H \gtrsim m_{H^\pm} + m_W$ (such that $H \rightarrow H^\pm W^\mp$ is kinematically allowed, but nevertheless phase space suppressed). The phenomenology of this kind of scenario is however largely contained in Planes I-II, and so we do not consider it separately.

^{¶¶} $t_\beta \neq 1$ is chosen for the exotic decays into two lighter new scalars ($H \rightarrow AA$ in this case) not to vanish.

- BP IIB: $m_H < m_A = m_{H^\pm}$.

As for BP IA, we consider Case 1 with $t_\beta = 1.5, 7, 30$ and Case 2 with $t_\beta = 1.5$.

In order to study the decays of the new scalars into the SM-like Higgs, we also consider a plane in which the departure from alignment is explored, assuming h is the 125 GeV SM-like Higgs (Plane III). We set $m_H = m_A = m_{H^\pm}$ for simplicity, and define the plane as $m_H = m_A = m_{H^\pm}$ vs. $c_{\beta-\alpha}$:

Plane III: $m_A = m_H = m_{H^\pm}$ vs. $c_{\beta-\alpha}$

- BP III:

We consider Case 1 with $t_\beta = 1.5, 7, 30$ and Case 2 with $t_\beta = 1.5$.

A summary of the different benchmark planes considered and the relevant exotic decay modes is shown in Table 3. In all cases, we present the $\sigma \times$ BR of each characteristic decay channel at the 13 TeV LHC, together with a detailed analysis of the regions disfavoured by theoretical and experimental constraints (including flavour constraints, shown for reference only). The results for Planes I and II ($c_{\beta-\alpha} = 0$) are presented in Section 5.1, while the results for decays to SM-like Higgs away from alignment, corresponding to Plane III, are presented in Section 5.2. Further details on the cross sections and decay branching fractions for the non-SM like Higgses can be found in Appendix A.

| | Mass Planes | decays | m_{12}^2 | $\tan \beta$ | Figures |
|--------|---|--|-------------------------|--------------|------------|
| BP IA | $m_A > m_H = m_{H^\pm}$ | $A \rightarrow H^\pm W^\mp$ | $m_H^2 s_\beta c_\beta$ | 1.5, 7, 30 | 5, 6 |
| | | $A \rightarrow HZ$ | 0 | 1.5 | |
| BP IB | $m_A < m_H = m_{H^\pm}$ | $H \rightarrow AZ, H \rightarrow AA$ $H^\pm \rightarrow AW^\pm$ | 0 | 1.5 | 9 |
| BP IIA | $m_H > m_A = m_{H^\pm}$ | $H \rightarrow AZ, H \rightarrow AA$ $H \rightarrow H^+ H^-, H \rightarrow H^\pm W^\mp$ | 0 | 1.5 | 10 |
| BP IIB | $m_H < m_A = m_{H^\pm}$ | $A \rightarrow HZ$ | $m_H^2 s_\beta c_\beta$ | 1.5, 7, 30 | 7, 8 |
| | | $H^\pm \rightarrow HW^\pm$ | 0 | 1.5 | |
| BP III | $m_A = m_H = m_{H^\pm}$ vs. $c_{\beta-\alpha}$ | $A \rightarrow hZ, H^\pm \rightarrow hW^\pm$ | $m_H^2 s_\beta c_\beta$ | 1.5, 7, 30 | 11, 12, 13 |
| | | $H \rightarrow hh$ | 0 | 1.5 | |

Table 3. Summary Table of the different 2HDM benchmark planes.

Before we move on to discuss in detail our different 2HDM planes for LHC searches at 13 TeV, let us comment on the comparison of these benchmark scenarios with others proposed in the literature. In particular, our Planes I and II have a substantial overlap with the 2HDM “*short cascade*” scenario D from [64], while our specific BP IA and BP IIB have similarities with the $A \rightarrow HZ$ benchmarks for $c_{\beta-\alpha} = 0$ in [15] (see also [18]). As compared to [64], the present analysis explores the full mass plane, not restricted to specific

benchmark lines with fixed relations*** among m_H , m_A and m_{H^\pm} . We also explore the dependence on t_β , which has a significant impact on the allowed 2HDM parameter space for Planes I and II. Moreover, our analysis includes the 8 TeV experimental constraint from the CMS $H \rightarrow AZ/A \rightarrow HZ$ search [22, 23], precisely tailored to probe these 2HDM scenarios and thus a key ingredient in a study of 2HDM exotic Higgs decays.

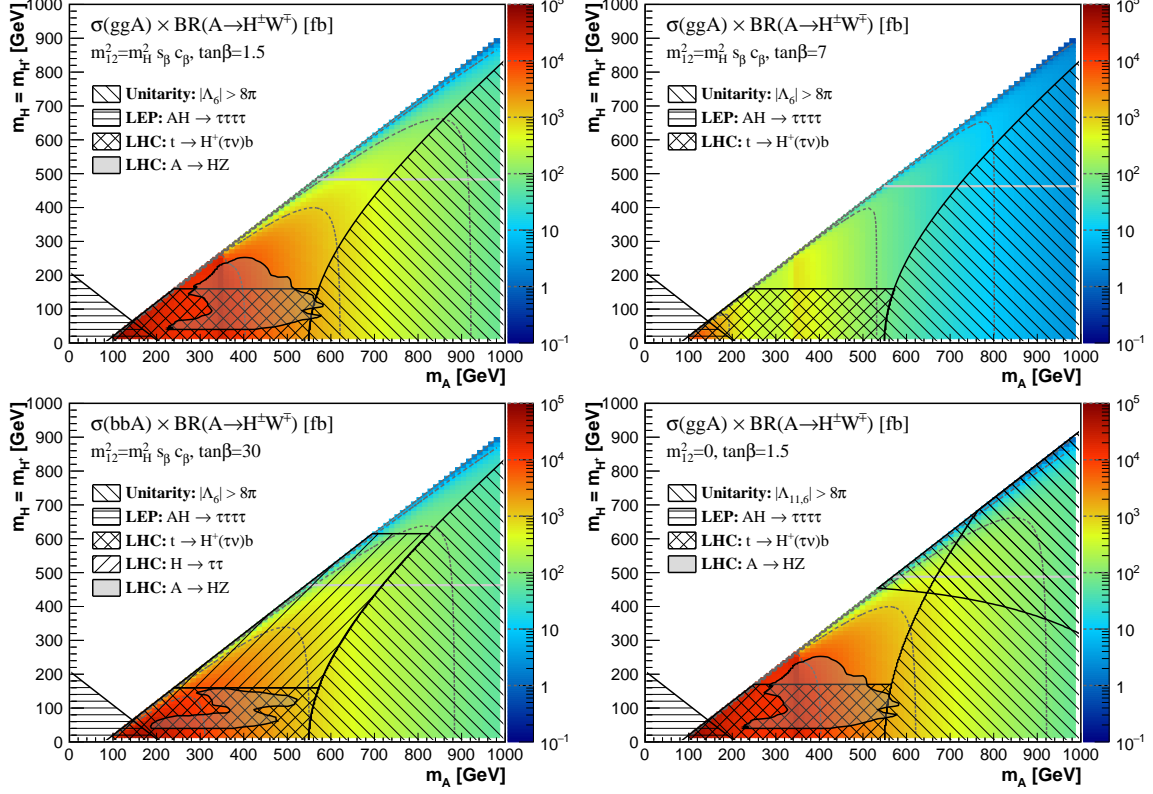


Figure 5. $\sigma \times \text{BR}$ for the exotic decay $A \rightarrow H^\pm W^\mp$ in BP IA: m_A vs $m_H = m_{H^\pm}$ plane, for Case 1 with $t_\beta = 1.5$ (upper left), 7 (upper right), 30 (lower left) and Case 2 with $t_\beta = 1.5$ (lower right). Contour lines of 10, 10^2 , 10^3 and 10^4 fb are drawn as light grey dashed curves to guide the eye. The shaded areas enclosed by an irregular curve and hatched regions are ruled out by theoretical and experimental constraints (see text for details). The solid horizontal grey line indicates the flavour constraint $m_{H^\pm} > 480$ GeV.

It is worth discussing here the extent to which a departure from our Benchmark Plane assumptions (Case 1 with $m_{12}^2 = m_H^2 s_\beta c_\beta$ or Case 2 with $m_{12}^2 = 0$, with certain mass degeneracy relations between m_A , m_H and m_{H^\pm}) may lead to modifications of the 2HDM phenomenology w.r.t. the scenarios we consider in this work:

- **Negative m_{12}^2 :** Extending m_{12}^2 to be negative does not introduce further constraints regarding vacuum stability. In addition, the variation of unitarity constraints for $m_{12}^2 < 0$ w.r.t. the $m_{12}^2 = 0$ case is mild, such that $m_{12}^2 = 0$ effectively captures this scenario.

***In particular, we note that the fixed relations in [64] result in the exotic Higgs decays being largely subdominant above the $t\bar{t}$ threshold, which may not be the case in general (see e.g. Figure 4).

- **Deviation from $m_{12}^2 = m_H^2 s_\beta c_\beta$:** Assuming the alignment limit $c_{\beta-\alpha} = 0$, at high t_β the soft \mathbb{Z}_2 breaking term m_{12}^2 is fixed to be around $m_H^2 s_\beta c_\beta$ by unitarity. Only when departing significantly from the alignment limit are deviations from $m_{12}^2 = m_H^2 s_\beta c_\beta$ at high t_β possible, yielding a larger allowed region in parameter space.

At low values of t_β deviations from $m_{12}^2 = m_H^2 s_\beta c_\beta$ can be easily accommodated in the alignment limit. We however stress that changing the value of m_{12}^2 only affects cubic and quartic Higgs couplings. In particular, HH^+H^- and HAA coupling vanish for $m_{12}^2 = m_H^2 s_\beta c_\beta$ in the alignment limit (see Section 3.6). Deviations from $m_{12}^2 = m_H^2 s_\beta c_\beta$ will then increase the branching fractions of $H \rightarrow AA$ and $H \rightarrow H^+H^-$ (if allowed by kinematics) with the branching fractions to other final states decreasing accordingly. For m_{12}^2 far away from $m_H^2 s_\beta c_\beta$, the branching fraction dependence on m_{12}^2 is mild, with Case 2 ($m_{12}^2 = 0$) being a representative scenario.

- **Deviations from the alignment limit $c_{\beta-\alpha} = 0$:** In our discussion we mainly focus on the alignment limit, preferred by Higgs coupling measurements at the LHC. In particular, we find that in the alignment limit, unitarity and vacuum stability cannot be satisfied simultaneously if $m_H > m_A$ or m_{H^\pm} at high t_β and therefore decays of the type $H \rightarrow AZ$, $H \rightarrow H^\pm W^\mp$ are not permitted for large t_β . This statement can be relaxed when deviating from the alignment limit. For moderate values of $|c_{\beta-\alpha}|$ around 0.2–0.6, there are regions of parameter space with $m_H > m_A$, m_{H^\pm} , which are allowed by both unitarity and vacuum stability. Note however that once away from the alignment limit, channels like $H \rightarrow AZ$, $H^\pm W^\mp$ will generically have reduced branching fractions. There have been studies in the literature for exotic Higgs decays in those non-alignment region [18, 65, 66].
- **Deviation from mass degeneracy:** The mass degeneracy relation is mainly imposed by the electroweak precision measurements. As shown in the left panel of Fig. 2, small deviations from $m_{H^\pm} \approx m_{A/H}$ are allowed. In principle, there are small regions of parameter space corresponding to a mass hierarchy $m_H = m_A < m_{H^\pm}$. However, these region of parameter space are already in almost 2σ tension with observation. Other deviations from mass degeneracy will not lead to a phenomenology that would differ significantly from that of BP I and BP II.

5.1 Exotic Decays in the Alignment Limit

5.1.1 BP IA: $m_A > m_H = m_{H^\pm}$

In this scenario, and for a sufficient mass splitting, there are two dominant exotic decay channels: $A \rightarrow H^\pm W^\mp$ and $A \rightarrow HZ$, for which we respectively show the $\sigma \times \text{BR}$ in Figures 5 and 6. In each case, we show four panels corresponding to the choices of m_{12}^2 and t_β described in Table 3. Note that for $t_\beta = 1.5, 7$ we consider the dominant ggA production, while for $t_\beta = 30$ the bbA production dominates and is considered instead. For each panel, contour lines of 10, 10^2 , 10^3 and 10^4 fb are drawn as light grey dashed curves to guide the eye. Large cross sections $\sigma \times \text{BR} \gtrsim 1$ pb are possible for $t_\beta \sim 1$ and $t_\beta \gg 1$, respectively due to the enhanced top and bottom Yukawa coupling contribution,

even for large CP-odd scalar masses $m_A \sim 500 - 600$ GeV. The shaded areas enclosed by an irregular curve in Figures 5 and 6 are excluded by the CMS $A \rightarrow HZ$ search [22, 23], which already constrains a sizable portion of parameter space and highlights the potential of such a search at LHC 13 TeV in the $b\bar{b}\ell\ell$ and $\tau\tau\ell\ell$ final states, as a probe of both A and H .

Hatched regions show the parameter space excluded by other experimental searches, as well as unitarity constraints. The former exclusions are mainly due to $t \rightarrow H^+b$ searches, which yield a limit $m_{H^\pm} > m_t$, as well as $H \rightarrow \tau\tau$ searches for large t_β , which rule out $m_H < 600$ GeV for $t_\beta = 30$. We also show the flavour bound $m_{H^\pm} > 480$ GeV as a horizontal grey line for indicative purposes.

Regarding unitarity, for Case 1 ($m_{12}^2 = m_H^2 s_\beta c_\beta$) with $m_A > m_H = m_{H^\pm}$ the eigenvalues of the scattering matrix are $|\Lambda_{i \neq 6}|v^2 = m_A^2 - m_H^2 \pm \mathcal{O}(m_h^2)$ and $|\Lambda_6|v^2 = 5(m_A^2 - m_H^2) + m_h^2$. The latter imposes the strongest constraint, which rules out regions with a very large mass splitting $m_A - m_H$ (as indicated by the hatched region in the lower-right corner of each panel in Figures 5 and 6). For Case 2 ($m_{12}^2 = 0$) with $m_A > m_H = m_{H^\pm}$, the strongest unitarity constraints come from $|\Lambda_6|v^2 = 5m_A^2 - 3m_H^2 \pm \mathcal{O}(m_h^2)$ and $|\Lambda_{11}|v^2 = \frac{1}{2}m_H^2(\frac{1}{t_\beta^2} + t_\beta^2) + \frac{1}{2}\sqrt{9m_H^4(\frac{1}{t_\beta^2} - t_\beta^2)^2 + 4m_A^4} \pm \mathcal{O}(m_h^2)$. In particular, $|\Lambda_{11}|$ rules out the large m_H region (upper hatched region in the lower right panel in Figures 5 and 6).

Taking into account both the theoretical and experimental constraints, relatively large regions of m_A vs. $m_H = m_{H^\pm}$ remain viable and having a sizable signal cross section for small to intermediate values of t_β for Case I. For $t_\beta \gg 1$, only the region $m_A \gtrsim m_H = m_{H^\pm} > 600$ GeV still survives. For Case 2, given the unitary constraints ruling out large values of m_H and m_A , only the region $200 \text{ GeV} < m_A < 650 \text{ GeV}$ and $175 \text{ GeV} < m_H = m_{H^\pm} < 450 \text{ GeV}$ remains viable.

5.1.2 BP IIB: $m_H < m_A = m_{H^\pm}$

For $m_H < m_A = m_{H^\pm}$, the dominant exotic decay channels are $A \rightarrow HZ$ and $H^\pm \rightarrow HW^\pm$. We show the $\sigma \times \text{BR}$ for $A \rightarrow HZ$ and $H^\pm \rightarrow HW^\pm$ respectively in Figures 7 and 8. The low $m_A + m_H$ region is ruled out by the LEP search $e^+e^- \rightarrow AH$ (recall the discussion in Section 3.5), while unitarity constraints bound large values for m_A, m_H : For Case I the strongest constraints arise from $|\Lambda_{2,4,5,6,11,12}|v^2 = 3(m_A^2 - m_H^2) \pm \mathcal{O}(m_h^2)$, which limit $m_A^2 - m_H^2$ for large m_H and/or m_A . For Case 2, large values of either m_A or m_H are excluded, since the strongest unitarity constraint comes from $|\Lambda_{11}|v^2 = \frac{1}{2}m_H^2(\frac{1}{t_\beta^2} + t_\beta^2) + \frac{1}{2}\sqrt{9m_H^4(\frac{1}{t_\beta^2} - t_\beta^2)^2 + 4(3m_A^2 - 2m_H^2)^2} \pm \mathcal{O}(m_h^2)$.

For Case 1 with $t_\beta = 1.5$ (upper left panel of Figure 7), signal cross sections for $A \rightarrow HZ$ in excess of 10 pb are viable given all the constraints, while we note that the LHC Run 1 CMS $A \rightarrow HZ$ search rules out a large portion of the parameter space with $m_H < 300$ GeV and $m_A < 650$ GeV. Intermediate values of t_β (exemplified by the $t_\beta = 7$ case shown in the upper right panel of Figure 7) only permit signal cross sections below 1 pb, due to the small gluon fusion production cross section (for $m_A > 600$ GeV the $\sigma \times \text{BR}$ values are in fact below 20 fb). For $t_\beta = 30$ (lower left panel of Figure 7), the current collider search of $H \rightarrow \tau\tau$ rules out $m_H < 600$ GeV, leaving only a small corner

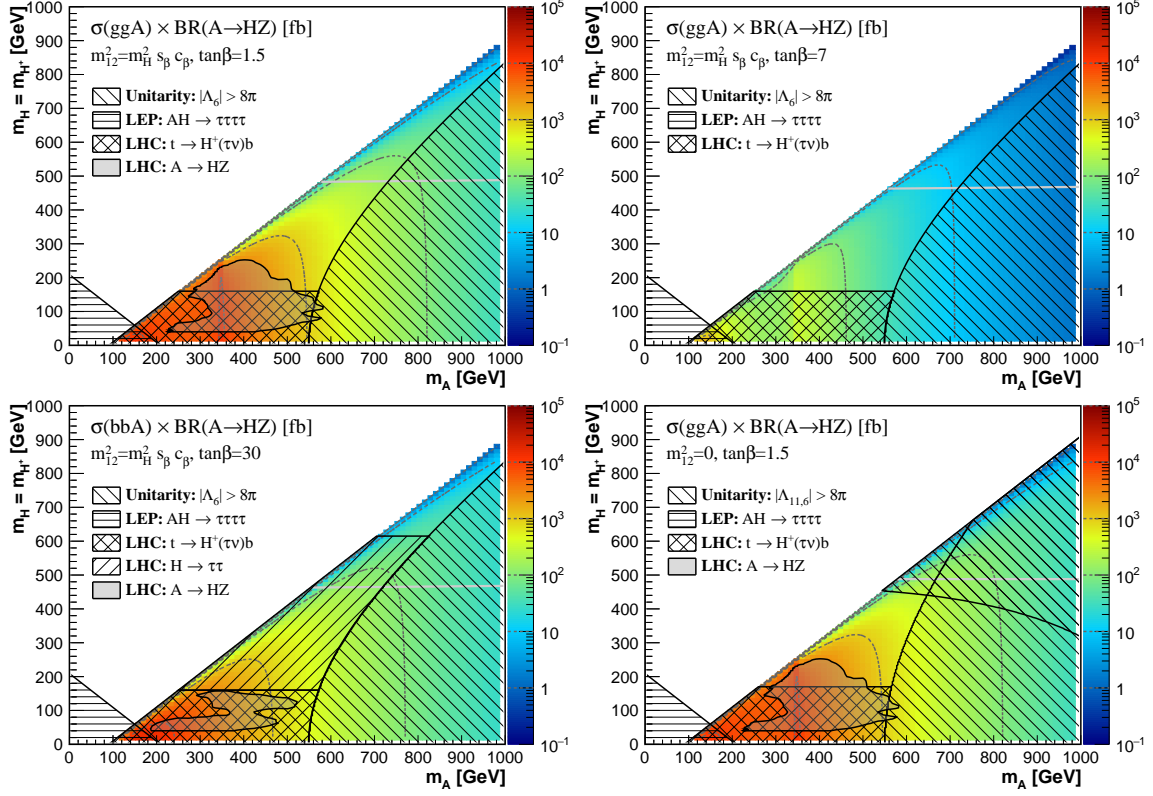


Figure 6. $\sigma \times \text{BR}$ for the exotic decay $A \rightarrow HZ$ in BP IA: m_A vs $m_H = m_{H^\pm}$ plane (see caption of Figure 5 for further details). For $t_\beta = 1.5$, the contour line at $\sigma \times \text{BR} = 10$ pb around $m_A = 350$ GeV is caused by the enhanced $gg \rightarrow A$ production cross section at the top threshold.

of parameter space allowed, with signal cross sections $\sigma \times \text{BR} \lesssim 100$ fb. For Case 2, the lower right panel of Figure 7 shows that the CMS $A \rightarrow HZ$ search constrains most of the viable parameter space, which may in turn be probed completely by LHC 13.

While the generic features for $H^\pm \rightarrow HW^\pm$ are similar to those of $A \rightarrow HZ$, the signal cross sections are about two order of magnitude smaller, due to the suppressed production cross section of $pp \rightarrow H^\pm tb$. This, in addition to the complicated final state HW^+W^-bb which results, makes this channel challenging for LHC studies at 13 TeV.

5.1.3 BP IB: $m_A < m_{H^\pm} = m_H$

In this scenario, only Case 2 ($m_{12}^2 = 0$) is viable. The $\sigma \times \text{BR}$ for the three possible exotic decay channels $H \rightarrow AZ$, $H^\pm \rightarrow AW^\pm$ and $H \rightarrow AA$ is shown in Figure 9 for our benchmark $t_\beta = 1.5$. The $m_H > 460$ GeV region is excluded by unitarity, the strongest unitarity constraint coming from $|\Lambda_{11}|v^2 = \frac{1}{2}m_H^2(\frac{1}{t_\beta^2} + t_\beta^2) + \frac{1}{2}\sqrt{9m_H^4(\frac{1}{t_\beta^2} - t_\beta^2)^2 + 4m_A^4} \pm \mathcal{O}(m_h^2)$.

Below the unitarity limit on m_H , the ATLAS/CMS limits on $A \rightarrow \tau\tau$ at low t_β (ggA production) [46, 47] combined with the bounds from the CMS $H \rightarrow AZ$ search [22, 23] rule out $m_A > 40$ GeV down to $m_H \lesssim 350$ GeV. As can be seen from Figure 9, only a small region of parameter space survives the unitarity and LHC 8 TeV constraints. We

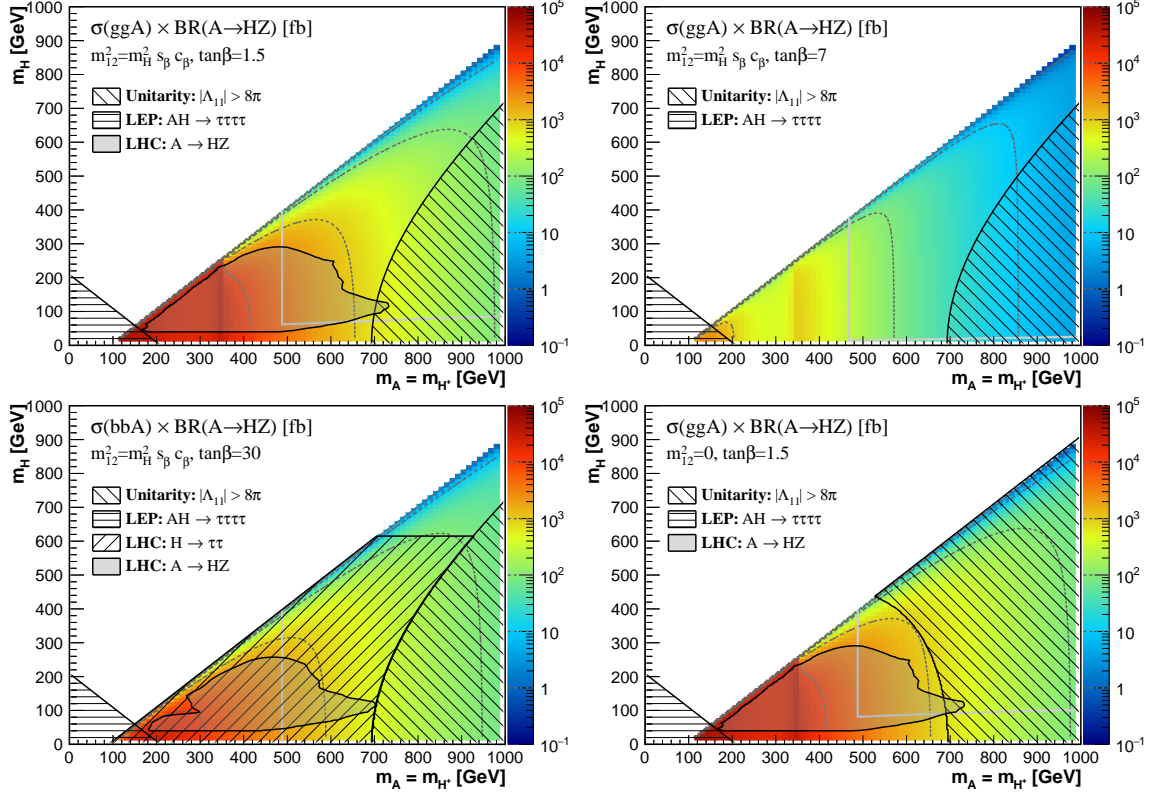


Figure 7. $\sigma \times \text{BR}$ for the exotic decay $A \rightarrow HZ$ in BP IIB: $m_A = m_{H^\pm}$ vs m_H plane (see caption of Figure 5 for further details). The solid horizontal and vertical light grey lines indicate the various flavour constraints.

also stress that in this case including the flavour constraint $m_{H^\pm} > 480$ GeV would rule out this benchmark scenario completely.

5.1.4 BP IIA: $m_H > m_A = m_{H^\pm}$

Four exotic Higgs decay channels, $H \rightarrow AZ$, $H \rightarrow H^\pm W^\mp$, $H \rightarrow AA$, and $H \rightarrow H^+ H^-$ are possible for BP IIA (which we recall is only allowed for Case 2), shown respectively in the four panels of Figure 10. Comparing to BP IIB, the additional collider search limit $m_{H^\pm} > m_t$ applies, which overlaps with the 8 TeV LHC exclusion from $A \rightarrow \tau\tau$. This results in only a small stripe in parameter space, corresponding to $200 \text{ GeV} < m_A = m_{H^\pm} < 240 \text{ GeV}$ and $300 \text{ GeV} < m_H < 450 \text{ GeV}$, being viable. Moreover, we note that the decays $H \rightarrow AA$ and $H \rightarrow H^+ H^-$ are essentially not kinematically allowed in the viable region, as shown in the lower panels of Figure 10. This benchmark scenario should indeed be possible to probe completely at LHC 13 TeV.

5.2 Exotic Decays into h Away from Alignment

5.2.1 BP III: $m_A = m_H = m_{H^\pm}$ vs. $c_{\beta-\alpha}$

Exotic decays with the SM-like Higgs h in the final state are possible away from the alignment limit $c_{\beta-\alpha} = 0$, as the AhZ , $H^\pm h W^\mp$ and Hhh couplings are proportional to

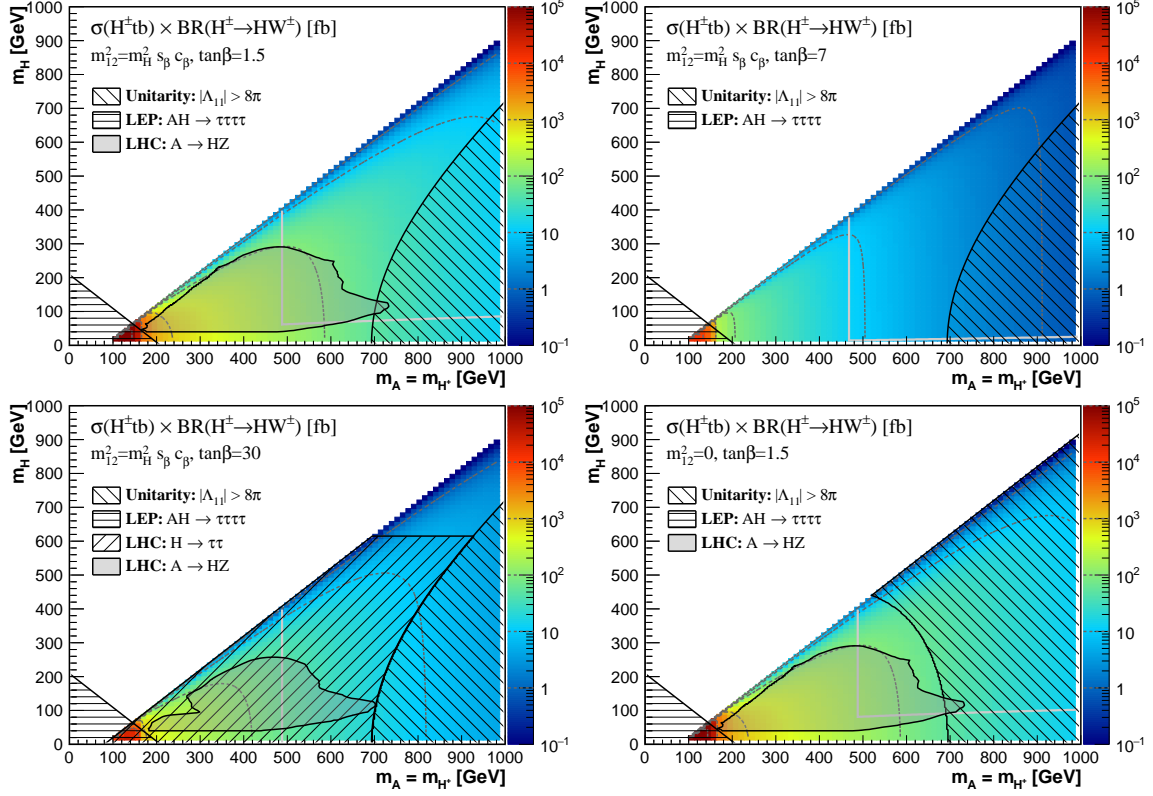


Figure 8. $\sigma \times \text{BR}$ for the exotic decay $H^\pm \rightarrow HW^\pm$ in BP IIB: $m_A = m_{H^\pm}$ vs. m_H plane (see caption of Figure 5 for further details). The solid horizontal and vertical light grey lines indicate the various flavour constraints.

$c_{\beta-\alpha}$. In Figures 11, 12, and 13 we respectively show the $\sigma \times \text{BR}$ for $A \rightarrow hZ$, $H^\pm \rightarrow hW^\pm$ and $H \rightarrow hh$, in each case for Case 1 with $t_\beta = 1.5, 7, 30$ and Case 2 with $t_\beta = 1.5$ in the $(c_{\beta-\alpha} \text{ vs } m_A = m_H = m_{H^\pm})$ plane.

For Case 1 with $t_\beta = 1.5$, only the region $|c_{\beta-\alpha}| \lesssim 0.2$ (close to the alignment limit) is viable as a result of Higgs signal strength measurements (mainly driven by the g_{hVV} couplings) considering all the theoretical and experimental constraints. The allowed range for $c_{\beta-\alpha}$ shrinks as the masses of the heavy 2HDM scalars grow due to stability constraints, being already restricted to $-0.02 < c_{\beta-\alpha} < 0.06$ for $m_A = m_H = m_{H^\pm} \simeq 500$ GeV. At the same time, LHC bounds on $H \rightarrow ZZ$ and $A \rightarrow \tau\tau$ rule out $m_A = m_H = m_{H^\pm} < 350$ GeV. For significantly higher values of t_β (as our $t_\beta = 7, 30$ scenarios) the stability constraints rule out almost completely the region $c_{\beta-\alpha} < 0$, while unitarity imposes a strong constraint on $c_{\beta-\alpha} > 0$ for high scalar masses $m_A = m_H = m_{H^\pm} > 600$ GeV. In addition, for $t_\beta = 7$ the vacuum stability constraint rules out the region $c_{\beta-\alpha} > 0.3$ while Higgs signal strengths rule out the region $0.05 < c_{\beta-\alpha} < 0.24$. For $t_\beta = 30$, Higgs signal strengths rule out $c_{\beta-\alpha} \gtrsim 0.01$, while $A \rightarrow \tau\tau$ searches restrict the allowed parameter space to $m_A = m_H = m_{H^\pm} > 650$ GeV, leaving only a very narrow stripe as viable parameter space. For Case 2 with $t_\beta = 1.5$, satisfying the constraints from $H \rightarrow ZZ$ and $A \rightarrow \tau\tau$ requires $m_A = m_H = m_{H^\pm} > 350$ GeV and $|c_{\beta-\alpha}| \lesssim 0.2$, while unitarity imposes an

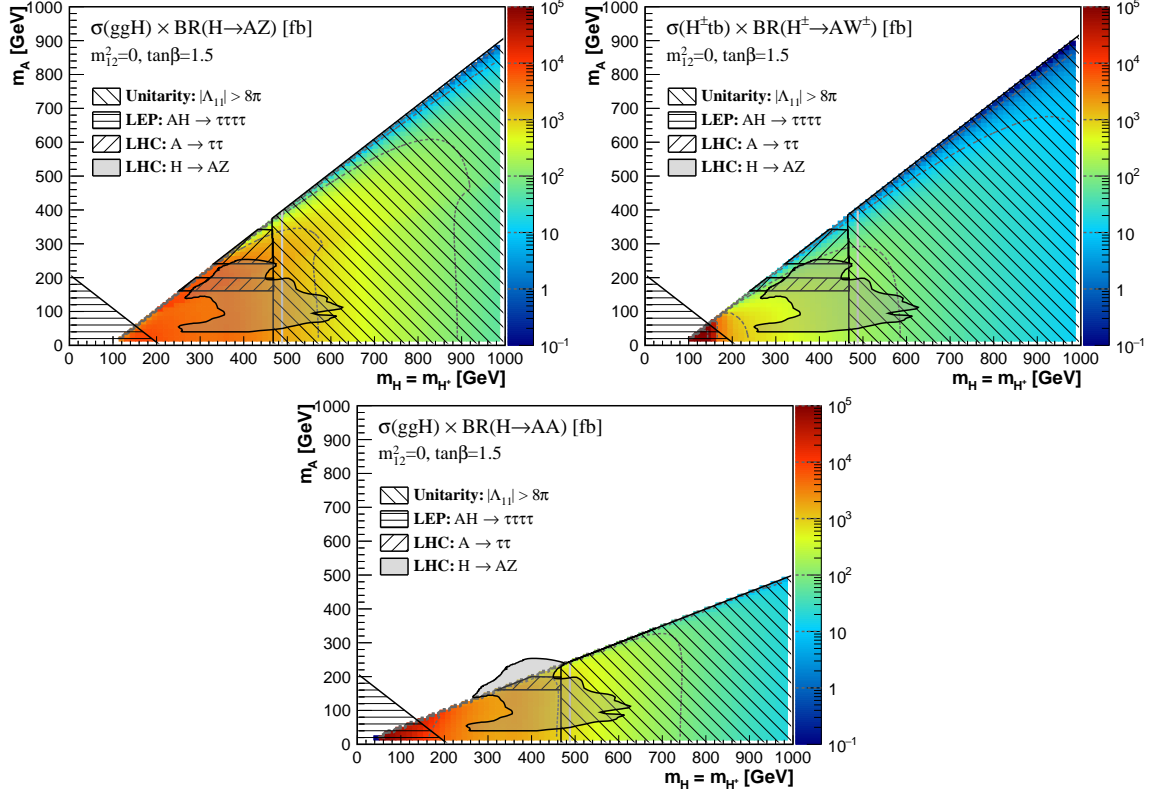


Figure 9. $\sigma \times \text{BR}$ for the exotic decays $H \rightarrow AZ$ (up left), $H^\pm \rightarrow AW^\pm$ (up right) and $H \rightarrow AA$ (down) in BP IB: $m_H = m_{H^\pm}$ vs. m_A plane, for Case 2 ($m_{12}^2 = 0$) with $t_\beta = 1.5$. Contour lines of 10, 10^2 and 10^3 fb are drawn as light grey dashed curves to guide the eye. The shaded areas enclosed by an irregular curve and hatched regions are ruled out by theoretical and experimental constraints (see text for details). The solid (vertical) light grey lines indicate the flavour constraint $m_{H^\pm} > 480$ GeV.

upper bound on the scalar masses in the range 450 GeV – 550 GeV depending on $c_{\beta-\alpha}$. As shown in Figure 11, the cross sections for $A \rightarrow hZ$ in the allowed region of parameter space could reach 1 pb or higher for $t_\beta = 1.5$ both in Case 1 and 2. For $t_\beta = 7$ (Case 1) the cross section for $A \rightarrow hZ$ is still sizable in the allowed region $0.24 < c_{\beta-\alpha} < 0.3$, reaching values ~ 100 fb. For $t_\beta = 30$ the signal cross section is however very small due to the suppressed branching ratio $\text{BR}(A \rightarrow hZ)$ close to the alignment limit. The signal cross sections for $H^\pm \rightarrow hW^\pm$ shown in Figure 12 follow a trend similar to those for $A \rightarrow hZ$, but being typically a factor 10 – 100 smaller due to the suppressed production cross section for H^\pm above m_t (see Appendix A.1). Finally for $H \rightarrow hh$ the signal cross sections, shown in Figure 13, are about factor of 10 smaller than those of $A \rightarrow hZ$, and an additional suppression of the branching ratio $\text{BR}(H \rightarrow hh)$ occurs for certain values of $c_{\beta-\alpha}$ (e.g. $c_{\beta-\alpha} \sim 0.22$ for $t_\beta = 7$ and $c_{\beta-\alpha} \sim 0.052$ for $t_\beta = 30$, as seen from Figure 13).

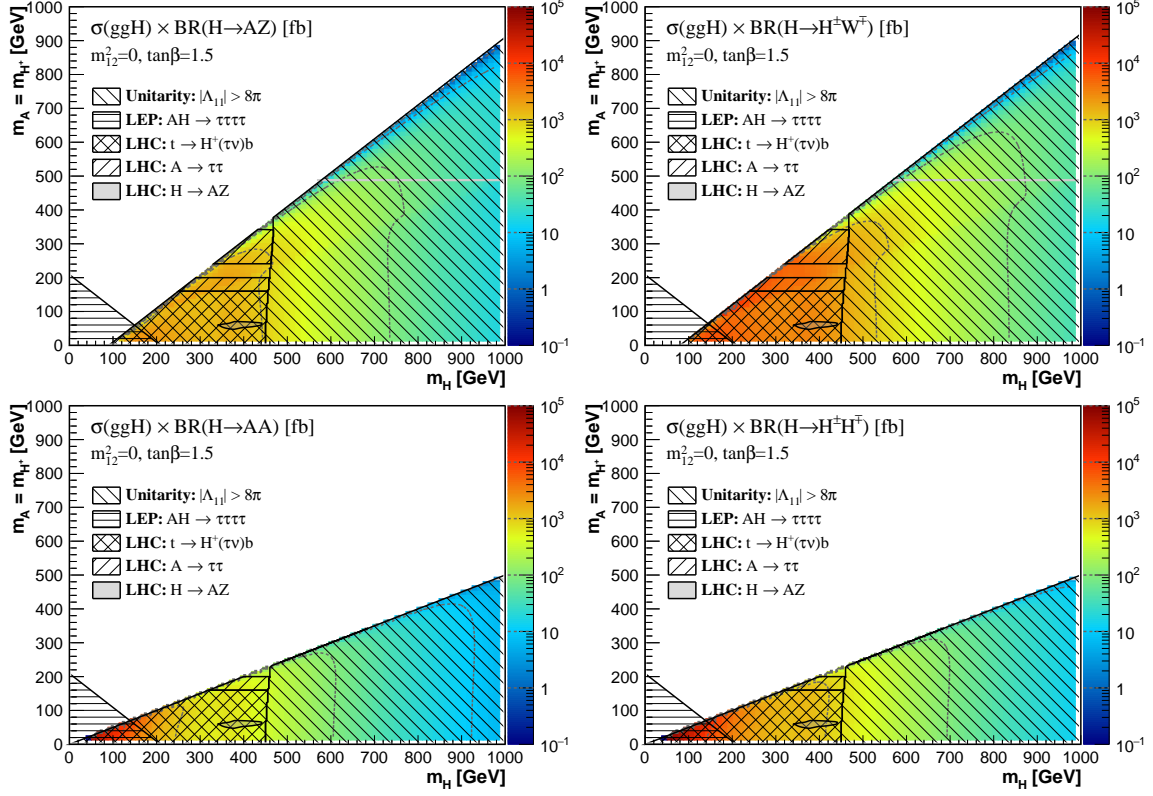


Figure 10. $\sigma \times \text{BR}$ for the exotic decays $H \rightarrow AZ$ (up left), $H^\pm \rightarrow H^\pm W^\mp$ (up right), $H \rightarrow AA$ (down left) and $H \rightarrow H^+ H^-$ (down right) in BP IIA: m_H vs. $m_A = m_{H^\pm}$ plane (see caption of Figure 9 for further details).

6 Conclusions

In the 2HDM, other than decaying to pairs of SM quarks, leptons, and gauge bosons, the exotic decays of heavy Higgses into two lighter Higgses or one light Higgs and a SM gauge boson are likely to dominate once they are kinematically open. While the collider search bounds for heavy Higgses based on conventional search modes WW , ZZ , $\gamma\gamma$, bb and $\tau\tau$ for neutral Higgses, and $\tau\nu$ and cs modes for charged Higgses would be relaxed once those exotic modes are open, the exotic decay modes offer new discovery channels in large regions of the 2HDM parameter space.

Away from the 2HDM alignment limit, exotic decays into the SM-like 125 GeV Higgs boson h , namely $H \rightarrow hh$, $A \rightarrow hZ$ and $H^\pm \rightarrow hW^\pm$, are potentially important, and there is already an ongoing ATLAS and CMS search programme for $A \rightarrow hZ$ [51, 52] and $H \rightarrow hh$ [53–55]. In contrast, close to the alignment limit, as favoured by measurements of Higgs signal strengths, exotic decays among the new 2HDM scalars become particularly relevant. The experimental searches based on those channels, however, have just started with $H/A \rightarrow AZ/HZ$ [22, 23]. In this work, we carefully examine the exotic Higgs decay channels in the 2HDM, both in the presence of a hierarchy between Higgses and away from alignment when this hierarchy is not present. By taking into account the various

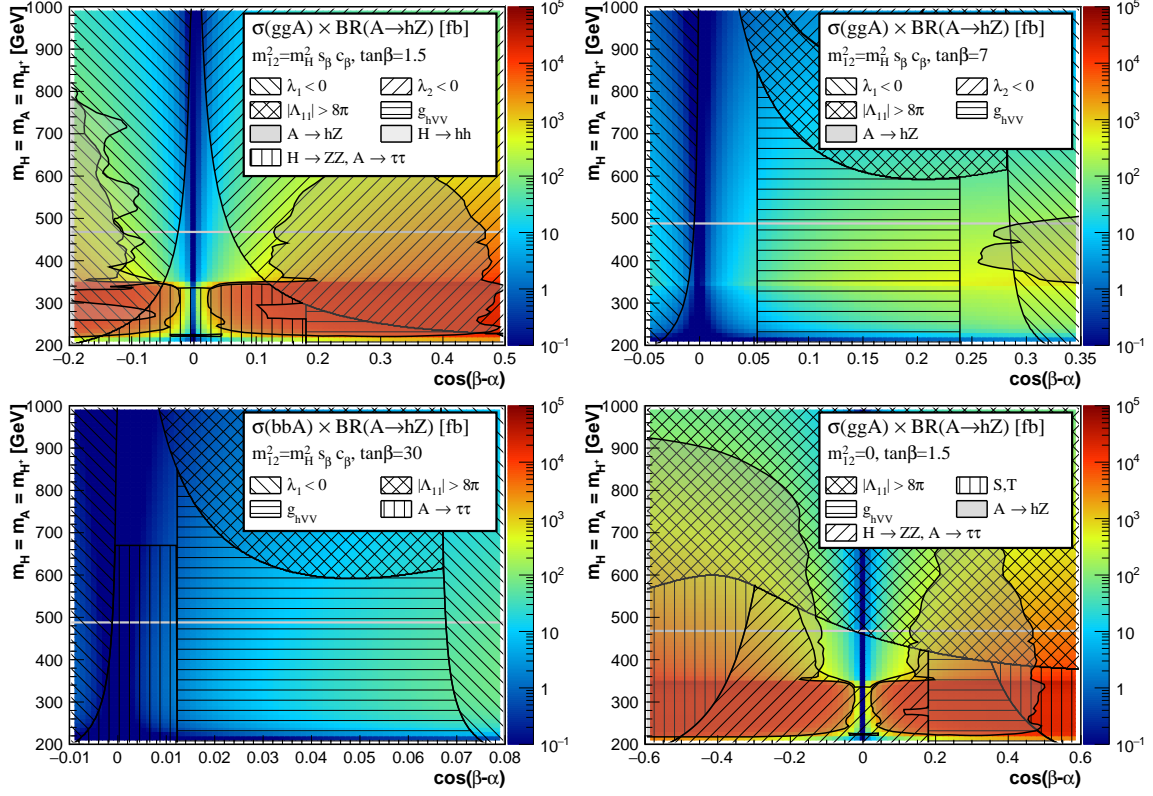


Figure 11. $\sigma \times \text{BR}$ for $A \rightarrow hZ$ for the gluon fusion production in Case 1, $\tan \beta = 1.5$ (upper left), 7 (upper right), as well as Case 2, $\tan \beta = 1.5$ (lower right), and bbA associated production for Case 1, $\tan \beta = 30$ (lower left) in BP III: $c_{\beta-\alpha}$ vs. $m_A = m_H = m_{H^\pm}$. Hatched regions are excluded by either theoretical or experimental constraints (as indicated in the legend), while the shaded areas enclosed by an irregular curve indicate the parameter space constrained by LHC searches for exotic (non-SM) Higgs decays: $A \rightarrow hZ$ and $H \rightarrow hh$. The solid horizontal light grey lines indicate the flavour constraint $m_{H^\pm} > 480$ GeV.

theoretical and experimental constraints, we propose 2HDM benchmark plane scenarios for LHC searches at 13 TeV:

- BP IA: $m_A > m_H = m_{H^\pm}$, with $A \rightarrow HZ$, $H^\pm W^\mp$.
- BP IB: $m_A < m_H = m_{H^\pm}$, with $H \rightarrow AZ$, AA and $H^\pm \rightarrow AW^\pm$.
- BP IIA: $m_H > m_A = m_{H^\pm}$, with $H \rightarrow AZ$, $H^\pm W^\mp$, AA , $H^+ H^-$.
- BP IIB: $m_H < m_A = m_{H^\pm}$, with $A \rightarrow HZ$ and $H^\pm \rightarrow HW^\pm$.
- BP III: $m_A = m_H = m_{H^\pm}$ vs. $c_{\beta-\alpha}$, with $A \rightarrow hZ$, $H^\pm \rightarrow hW^\pm$, and $H \rightarrow hh$.

In each case, we analyze the allowed regions of parameter space and the LHC 13 TeV $\sigma \times \text{BR}$ for the relevant exotic Higgs decay modes in those regions.

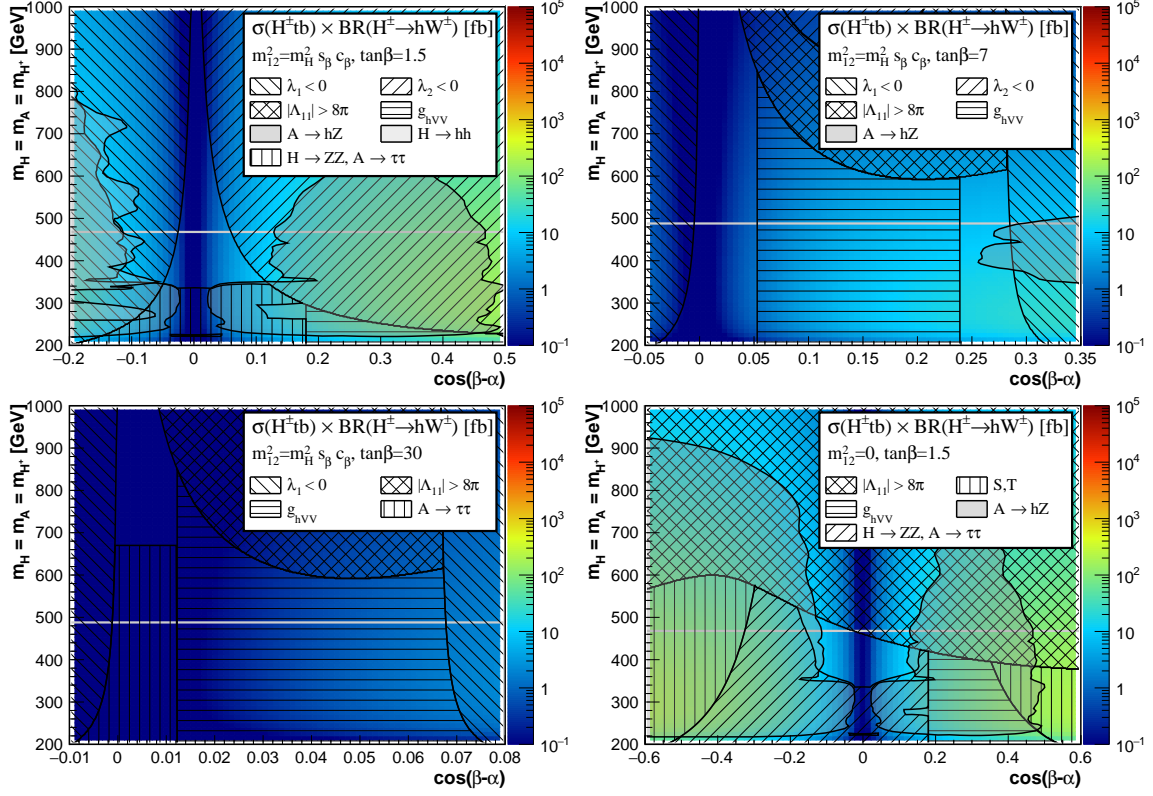


Figure 12. $\sigma \times \text{BR}$ for $H^\pm \rightarrow hW^\pm$ in BPIII: $c_{\beta-\alpha}$ vs. $m_A = m_H = m_{H^\pm}$ (see caption of Figure 11 for further details).

To summarize, exotic Higgs decays provide new discovery avenues for heavy Higgses. In turn, the exploration of the proposed benchmarks via these decays could help to understand the structure of the electroweak symmetry breaking sector beyond the SM.

Acknowledgments

We would like to thank Baradhwaj Coleppa, Tao Han, Tao Liu, Ken Mimasu and Adarsh Pyarelal for helpful discussions. We also thank the Munich Institute for Astro- and Particle Physics (MIAPP) of the DFG cluster of excellence “Origin and Structure of the Universe” for support and hospitality during the initial stages of this work. The work of S.S. and F.K. was supported by US Department of Energy under Grant DE-FG02-04ER-41298. F.K. also acknowledges support from the Fermilab Graduate Student Research Program in Theoretical Physics operated by Fermi Research Alliance, LLC under Contract No. DE-AC02-07CH11359 with the United States Department of Energy. J.M.N. is supported by the People Programme (Marie Curie Actions) of the European Union Seventh Framework Programme (FP7/2007-2013) under REA grant agreement PIEF-GA-2013-625809.

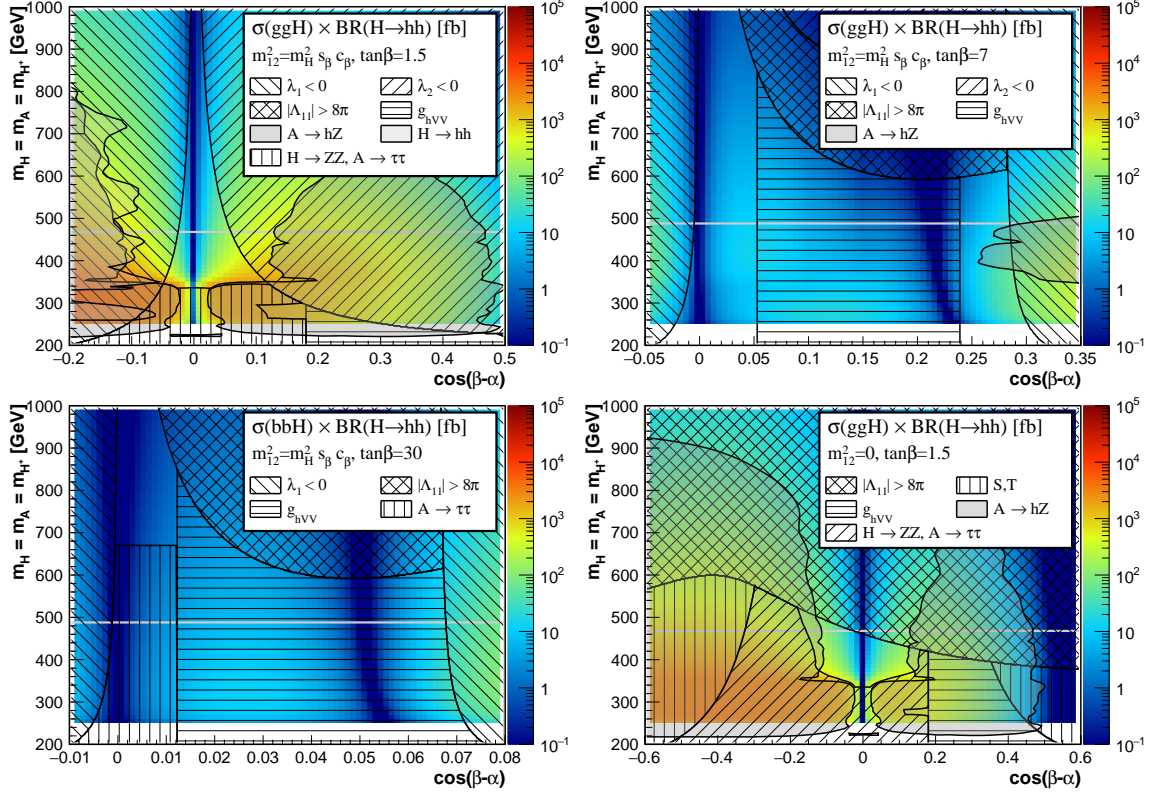


Figure 13. $\sigma \times \text{BR}$ for $H \rightarrow hh$ in BPIII: $c_{\beta-\alpha}$ vs. $m_A = m_H = m_{H^\pm}$ (see caption of Figure 11 for further details).

A Production Cross Sections and Branching Ratios of 2HDM Higgses

A.1 2HDM Production Cross Sections

In Figure 14, we show the gluon fusion production cross section for H (upper left panel) and A (upper right panel), bb -associated production cross section for H (middle left panel) and A (middle right panel), and tbH^\pm production cross section (bottom) for the charged scalar (details are given in Section 4).

A.2 2HDM Branching Ratios for Exotic Higgs Decays

For illustration, we show in Figure 15 the branching ratios of $H_a \rightarrow H_b V$ (with $H_{a,b} = H, A, H^\pm$ and $V = W^\pm, Z$) for Plane I (top) and Plane II (bottom) for Case 2 ($m_{12}^2 = 0$) with $t_\beta = 1.5$ (being the scenario allowed for the four benchmarks BP IA, BP IB, BP IIA and BP IIB). The decay branching ratios for $H/A \rightarrow AZ/H(h)Z$ are shown on the left panels of Figure 15, while those for $A/H^\pm \rightarrow H^\pm W^\mp/AW^\pm$ (Plane I) and $H/H^\pm \rightarrow H^\pm W^\mp/HW^\pm$ (Plane II) are shown on the right panels.

References

- [1] G. Aad *et al.* [ATLAS Collaboration], Eur. Phys. J. C **76** (2016) 1, 6 [arXiv:1507.04548 [hep-ex]].

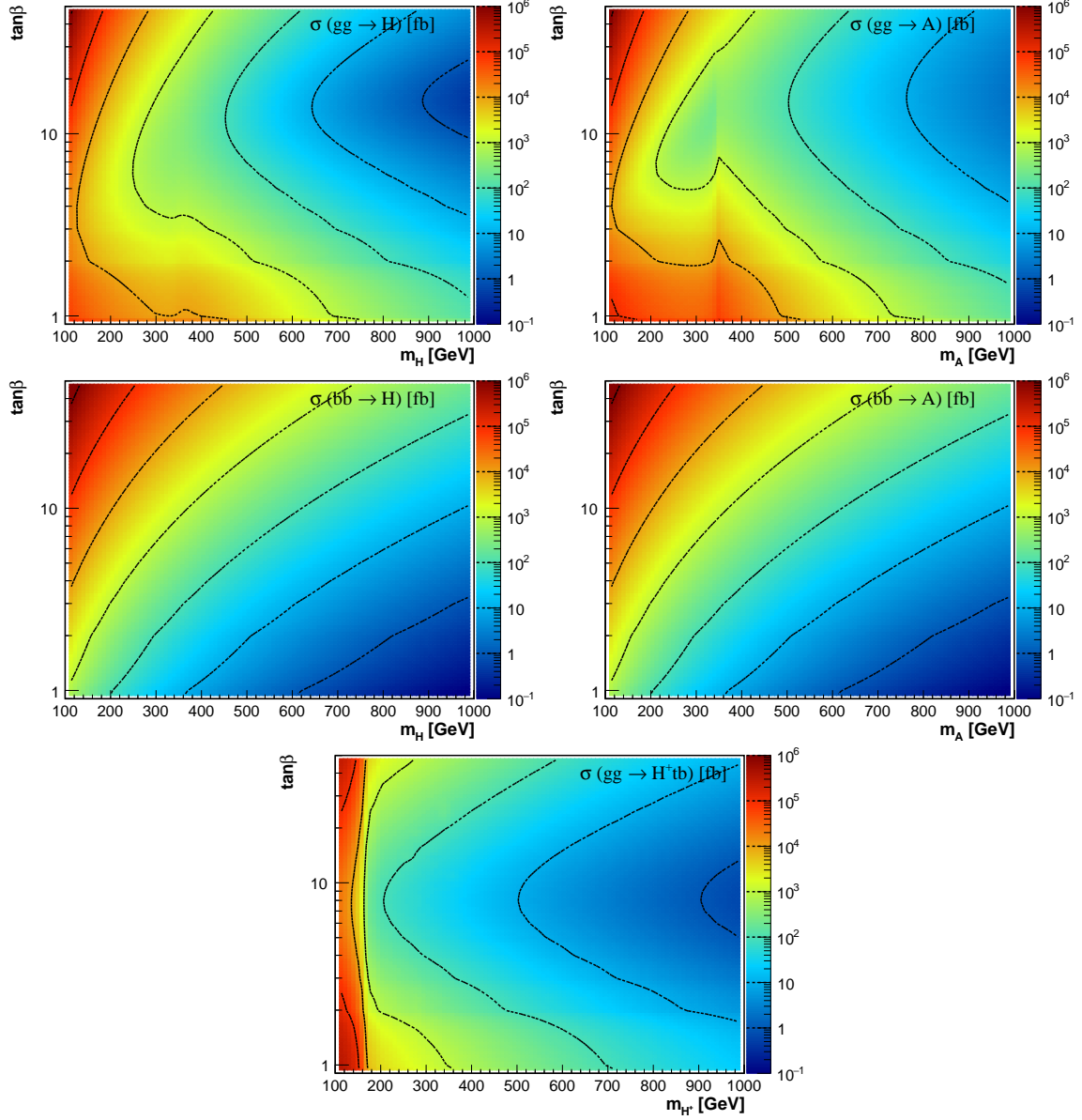


Figure 14. Production cross section for H , A and H^+ at LHC 13 TeV. The contour lines indicate the cross section of 1, 10, 10^2 , 10^3 , 10^4 , 10^5 and 10^6 fb.

- [2] V. Khachatryan *et al.* [CMS Collaboration], Eur. Phys. J. C **75** (2015) 5, 212 [arXiv:1412.8662 [hep-ex]].
- [3] A. Djouadi, Phys. Rept. **459** (2008) 1 [hep-ph/0503173].
- [4] J. Mrazek, A. Pomarol, R. Rattazzi, M. Redi, J. Serra and A. Wulzer, Nucl. Phys. B **853** (2011) 1 [arXiv:1105.5403 [hep-ph]]; E. Bertuzzo, T. S. Ray, H. de Sandes and C. A. Savoy, JHEP **1305** (2013) 153 [arXiv:1206.2623 [hep-ph]].
- [5] J. M. Cline, K. Kainulainen and A. P. Vischer, Phys. Rev. D **54** (1996) 2451 [hep-ph/9506284]; J. M. Cline and P. A. Lemieux, Phys. Rev. D **55** (1997) 3873 [hep-ph/9609240]; L. Fromme, S. J. Huber and M. Seniuch, JHEP **0611** (2006) 038

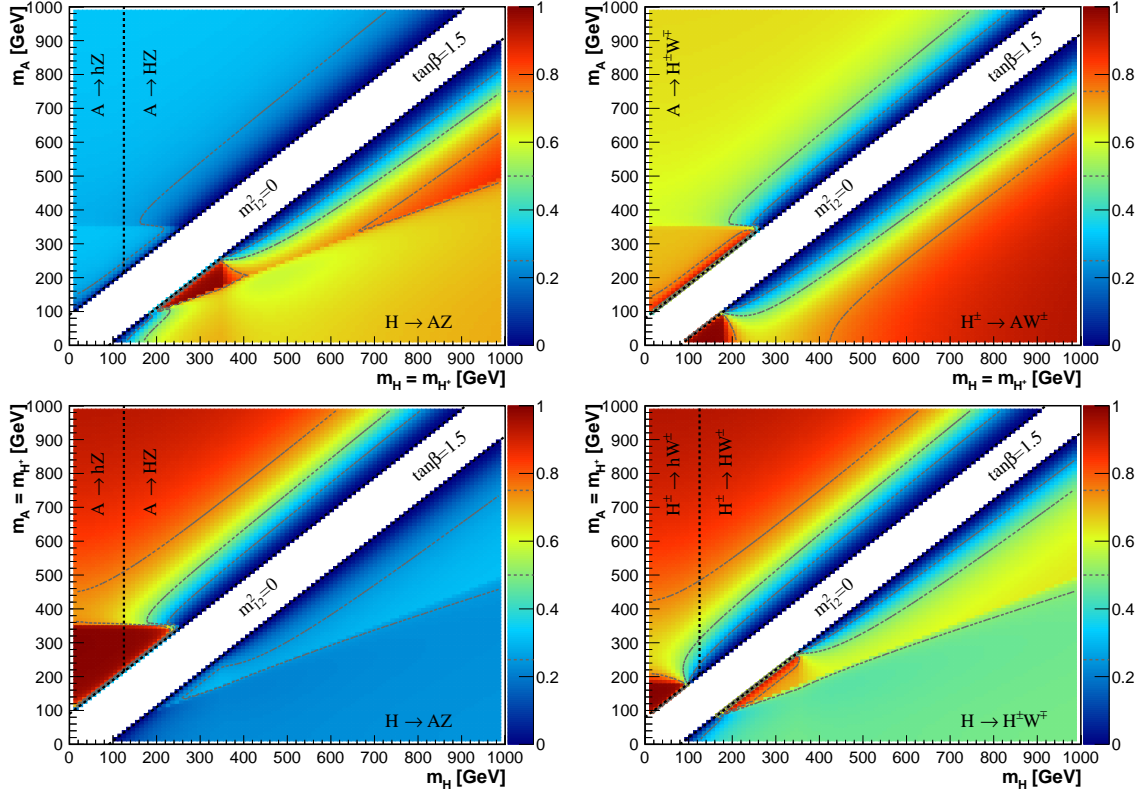


Figure 15. Left: Exotic decay BR $H/A \rightarrow AZ/H(h)Z$ for Plane I (top) and Plane II (bottom) for Case 2 ($m_{12}^2 = 0$) with $t_\beta = 1.5$. For $A \rightarrow H(h)Z$, we consider $A \rightarrow HZ$ for $m_H > m_h = 125$ GeV and $A \rightarrow hZ$ for $m_h < m_H = 125$ GeV (so that the BR into the non-SM like Higgs boson is shown in each case). Right: Exotic decay BR $A/H^\pm \rightarrow H^\pm W^\mp/AW^\pm$ for Plane I (top) and $H/H^\pm \rightarrow H^\pm W^\mp/HW^\pm$ for Plane II (bottom), for Case 2 ($m_{12}^2 = 0$) with $t_\beta = 1.5$.

[hep-ph/0605242]; G. C. Dorsch, S. J. Huber and J. M. No, JHEP **1310** (2013) 029 [arXiv:1305.6610 [hep-ph]].

- [6] A. Celis, V. Ilisie and A. Pich, JHEP **1307** (2013) 053 [arXiv:1302.4022 [hep-ph]].
- [7] B. Grinstein and P. Uttayarat, JHEP **1306** (2013) 094 [JHEP **1309** (2013) 110] [arXiv:1304.0028 [hep-ph]].
- [8] B. Coleppa, F. Kling and S. Su, JHEP **1401**, 161 (2014) [arXiv:1305.0002 [hep-ph]].
- [9] C. Y. Chen, S. Dawson and M. Sher, Phys. Rev. D **88** (2013) 015018 [Phys. Rev. D **88** (2013) 039901] [arXiv:1305.1624 [hep-ph]].
- [10] O. Eberhardt, U. Nierste and M. Wiebusch, JHEP **1307** (2013) 118 [arXiv:1305.1649 [hep-ph]].
- [11] B. Dumont, J. F. Gunion, Y. Jiang and S. Kraml, Phys. Rev. D **90** (2014) 035021 [arXiv:1405.3584 [hep-ph]].
- [12] J. Bernon, B. Dumont and S. Kraml, Phys. Rev. D **90** (2014) 071301 [arXiv:1409.1588 [hep-ph]].
- [13] N. Craig, F. D'Eramo, P. Draper, S. Thomas and H. Zhang, JHEP **1506** (2015) 137

- [arXiv:1504.04630 [hep-ph]].
- [14] J. Bernon, J. F. Gunion, H. E. Haber, Y. Jiang and S. Kraml, Phys. Rev. D **92** (2015) 7, 075004 [arXiv:1507.00933 [hep-ph]].
 - [15] G. C. Dorsch, S. J. Huber, K. Mimasu and J. M. No, arXiv:1601.04545 [hep-ph].
 - [16] B. Coleppa, F. Kling and S. Su, arXiv:1308.6201 [hep-ph].
 - [17] B. Coleppa, F. Kling and S. Su, JHEP **1409**, 161 (2014) [arXiv:1404.1922 [hep-ph]].
 - [18] G. C. Dorsch, S. J. Huber, K. Mimasu and J. M. No, Phys. Rev. Lett. **113** (2014) 21, 211802 [arXiv:1405.5537 [hep-ph]].
 - [19] B. Coleppa, F. Kling and S. Su, JHEP **1412**, 148 (2014) [arXiv:1408.4119 [hep-ph]].
 - [20] T. Li and S. Su, JHEP **1511** (2015) 068 [arXiv:1504.04381 [hep-ph]].
 - [21] F. Kling, A. Pyarelal and S. Su, JHEP **1511**, 051 (2015) [arXiv:1504.06624 [hep-ph]].
 - [22] CMS Collaboration [CMS Collaboration], CMS-PAS-HIG-15-001.
 - [23] V. Khachatryan *et al.* [CMS Collaboration], arXiv:1603.02991 [hep-ex].
 - [24] J. F. Gunion, H. E. Haber, G. L. Kane and S. Dawson, Front. Phys. **80**, 1 (2000).
 - [25] J. Bernon, J. F. Gunion, H. E. Haber, Y. Jiang and S. Kraml, arXiv:1511.03682 [hep-ph].
 - [26] J. F. Gunion and H. E. Haber, Phys. Rev. D **67**, 075019 (2003) [hep-ph/0207010].
 - [27] G. Abbiendi *et al.* [ALEPH and DELPHI and L3 and OPAL and LEP Collaborations], Eur. Phys. J. C **73** (2013) 2463 [arXiv:1301.6065 [hep-ex]].
 - [28] J. Bernon, J. F. Gunion, Y. Jiang and S. Kraml, Phys. Rev. D **91** (2015) 7, 075019 [arXiv:1412.3385 [hep-ph]].
 - [29] S. L. Glashow and S. Weinberg, Phys. Rev. D **15**, 1958 (1977).
 - [30] G. C. Branco, P. M. Ferreira, L. Lavoura, M. N. Rebelo, M. Sher and J. P. Silva, Phys. Rept. **516**, 1 (2012) [arXiv:1106.0034 [hep-ph]].
 - [31] G. Aad *et al.* [ATLAS Collaboration], JHEP **1511** (2015) 206 [arXiv:1509.00672 [hep-ex]].
 - [32] P. M. Ferreira, J. F. Gunion, H. E. Haber and R. Santos, Phys. Rev. D **89**, no. 11, 115003 (2014) [arXiv:1403.4736 [hep-ph]].
 - [33] I. F. Ginzburg and I. P. Ivanov, Phys. Rev. D **72** (2005) 115010 [hep-ph/0508020].
 - [34] B. Grinstein, C. W. Murphy and P. Uttayarat, arXiv:1512.04567 [hep-ph].
 - [35] M. Baak *et al.* [Gfitter Group Collaboration], Eur. Phys. J. C **74** (2014) 3046 [arXiv:1407.3792 [hep-ph]].
 - [36] M. Gorbahn, J. M. No and V. Sanz, JHEP **1510** (2015) 036 [arXiv:1502.07352 [hep-ph]].
 - [37] Y. Amhis *et al.* [Heavy Flavor Averaging Group (HFAG) Collaboration], arXiv:1412.7515 [hep-ex].
 - [38] F. Mahmoudi, Comput. Phys. Commun. **180** (2009) 1579 [arXiv:0808.3144 [hep-ph]].
 - [39] F. Mahmoudi, Comput. Phys. Commun. **180** (2009) 1718.
 - [40] J. P. Lees *et al.* [BaBar Collaboration], Phys. Rev. Lett. **109** (2012) 101802 [arXiv:1205.5442 [hep-ex]].

- [41] M. Huschle *et al.* [Belle Collaboration], Phys. Rev. D **92** (2015) no.7, 072014 [arXiv:1507.03233 [hep-ex]].
- [42] A. Abdesselam *et al.* [Belle Collaboration], arXiv:1603.06711 [hep-ex].
- [43] M. Misiak *et al.*, Phys. Rev. Lett. **114** (2015) 22, 221801 [arXiv:1503.01789 [hep-ph]].
- [44] T. Han, T. Li, S. Su and L. T. Wang, JHEP **1311**, 053 (2013) [arXiv:1306.3229 [hep-ph]].
- [45] S. Schael *et al.* [ALEPH and DELPHI and L3 and OPAL and LEP Working Group for Higgs Boson Searches Collaborations], Eur. Phys. J. C **47** (2006) 547 [hep-ex/0602042].
- [46] G. Aad *et al.* [ATLAS Collaboration], JHEP **1411** (2014) 056 [arXiv:1409.6064 [hep-ex]].
- [47] V. Khachatryan *et al.* [CMS Collaboration], JHEP **1410** (2014) 160 [arXiv:1408.3316 [hep-ex]].
- [48] [ATLAS Collaboration], ATLAS-CONF-2013-013.
- [49] G. Aad *et al.* [ATLAS Collaboration], Phys. Rev. D **92** (2015) 1, 012006 [arXiv:1412.2641 [hep-ex]].
- [50] V. Khachatryan *et al.* [CMS Collaboration], JHEP **1510** (2015) 144 [arXiv:1504.00936 [hep-ex]].
- [51] G. Aad *et al.* [ATLAS Collaboration], Phys. Lett. B **744** (2015) 163 [arXiv:1502.04478 [hep-ex]].
- [52] V. Khachatryan *et al.* [CMS Collaboration], Phys. Lett. B **748** (2015) 221 [arXiv:1504.04710 [hep-ex]].
- [53] G. Aad *et al.* [ATLAS Collaboration], Phys. Rev. Lett. **114** (2015) 8, 081802 [arXiv:1406.5053 [hep-ex]].
- [54] CMS Collaboration [CMS Collaboration], CMS-PAS-HIG-13-032.
- [55] V. Khachatryan *et al.* [CMS Collaboration], Phys. Lett. B **749** (2015) 560 [arXiv:1503.04114 [hep-ex]].
- [56] G. Aad *et al.* [ATLAS Collaboration], JHEP **1503** (2015) 088 [arXiv:1412.6663 [hep-ex]].
- [57] V. Khachatryan *et al.* [CMS Collaboration], JHEP **1511** (2015) 018 [arXiv:1508.07774 [hep-ex]].
- [58] D. Das and I. Saha, Phys. Rev. D **91**, no. 9, 095024 (2015) [arXiv:1503.02135 [hep-ph]].
- [59] D. Das, Int. J. Mod. Phys. A **30**, no. 26, 1550158 (2015) [arXiv:1501.02610 [hep-ph]].
- [60] R. V. Harlander, S. Liebler and H. Mantler, Comput. Phys. Commun. **184** (2013) 1605 [arXiv:1212.3249 [hep-ph]].
- [61] M. Flechl, R. Klees, M. Kramer, M. Spira and M. Ubiali, Phys. Rev. D **91**, no. 7, 075015 (2015) [arXiv:1409.5615 [hep-ph]]; S. Heinemeyer *et al.* [LHC Higgs Cross Section Working Group Collaboration], arXiv:1307.1347 [hep-ph]; S. Dittmaier, M. Kramer, M. Spira and M. Walser, Phys. Rev. D **83**, 055005 (2011) [arXiv:0906.2648 [hep-ph]]; E. L. Berger, T. Han, J. Jiang and T. Plehn, Phys. Rev. D **71**, 115012 (2005) [hep-ph/0312286].
- [62] M. Czakon and A. Mitov, Comput. Phys. Commun. **185**, 2930 (2014) [arXiv:1112.5675 [hep-ph]].
- [63] D. Eriksson, J. Rathsman and O. Stål, Comput. Phys. Commun. **181** (2010) 189 [arXiv:0902.0851 [hep-ph]].

- [64] H. E. Haber and O. Stål, Eur. Phys. J. C **75** (2015) no.10, 491 [arXiv:1507.04281 [hep-ph]].
- [65] C. Gao, M. A. Luty, M. Mulhearn, N. A. Neill and Z. Wang, arXiv:1604.03108 [hep-ph].
- [66] M. Bauer, M. Carena and K. Gemmler, JHEP **1511**, 016 (2015) [arXiv:1506.01719 [hep-ph]].